Obtuse Triangular Billiards I: Near the $(2, 3, 6)$ Triangle

Richard Evan Schwartz

CONTENTS

2000 AMS Subject Classification: 37E15

Keywords: billiards, obtuse triangles, periodic trajectories

Let S_ϵ denote the set of Euclidean triangles whose two small angles are within ϵ radians of $\frac{\pi}{6}$ and $\frac{\pi}{3}$ respectively. In this paper we prove two complementary theorems: (1) For any $\epsilon > 0$ there exists a triangle in S_ϵ that has no periodic billiard path of combinatorial length less than $1/\epsilon$. (2) Every triangle in $S_{1/400}$ has a periodic billiard path.

1. INTRODUCTION

Let T be a triangle—more precisely, a triangular region in the plane—with the shortest edge labeled 1, the next shortest edge labeled 2, and the longest edge labeled 3. A *billiard path* in T is an infinite polygonal path $\{s_i\} \subset T$, composed of line segments, such that each vertex $s_i \cap s_{i+1}$ lies in the interior of some edge of T, say the w_ith edge, and the angles that s_i and s_{i+1} make with this edge are complementary. (See [Gutkin 96], [Masur and Tabachnikov 02], and [Tabachnikov 95] for surveys on billiards.) The sequence $\{w_i\}$ is the *orbit type*. A periodic billiard path corresponds to a periodic orbit type. The *combinatorial length* of the periodic billiard path is the length of the minimal period of the orbit type.

In 1775 Fagnano proved that the combinatorial orbit 123 (repeating) describes a periodic orbit on every acute triangle. It is an exercise to show that 312321 (repeating) describes a periodic orbit on all right triangles. (See [Galperin et al. 91], [Hooper 06], [Holt 98], and [Troubetzkoy 04] for some deeper results on right-angled billiards.) A rational triangle, i.e., a triangle whose angles are all rational multiples of π, has a dense set of periodic billiard paths [Boshernitzyn et al. 98]. (See also [Masur 86].) The theory of rational billiards has deep connections to Riemann surface theory; see, for example, [Veech 92], and also the many references in [Masur and Tabachnikov 02].

In [Galperin et al. 91] and [Halbeisen and Hungerbuhler 00], some infinite families of periodic orbits that work for some obtuse irrational triangles are produced. Aside

1058-6458/2006 $0.50 per page
Experimental Mathematics **15**:2, page 161

from these results, very little is known about the obtuse (irrational) case of triangular billiards. The purpose of this paper is to point out some unexpected complexity in this case. We view this paper as an indication of the depth of the *triangular billiards problem*, a problem from the eighteenth century, which asks whether every triangle admits a periodic billiard path.

Pat Hooper and I wrote *McBilliards*,[1] a graphical user interface that searches for periodic billiard paths in triangles and then organizes the data in an efficient display. The results in this paper, and many of the ideas for the proofs, were discovered using McBilliards.

Let T_∞ denote the triangle whose jth angle is $j\pi/6$ for $j = 1, 2, 3$ and let S_ϵ denote the set of obtuse triangles T such that the jth angle of T is within ϵ radians of $j\pi/6$ for $j = 1, 2$. Thus triangles in S_ϵ are very close to T_∞ when ϵ is small. Here is our first result:

Theorem 1.1. *For any $\epsilon > 0$ there exists a triangle in S_ϵ that has no periodic billiard path of combinatorial length less than $1/\epsilon$.*

To complement Theorem 1.1 we prove the following theorem:

Theorem 1.2. *Every triangle in $S_{1/400}$ has a periodic billiard path.*

Theorem 1.2 is not optimal. Our point is just to get an effective estimate on the size of the neighborhood covered. Theorem 1.2 is the main step in proving that a triangle has a periodic billiard path provided that all its angles are at most 100 degrees. We have now completed the proof of this result. See [Schwartz 05a]. Also, we have written a Java applet [Schwartz 05b] that clearly illustrates both Theorem 1.2 and the 100-degree theorem. Using McBilliards, we can see that (probably) a triangle has a periodic billiard path if its angles are less than $5\pi/8$ (or 112.5 degrees), but beyond that we cannot yet decide.

In terms of the above result, T_∞ is unique among the right triangles. The right-angled isosceles triangle has the property that any obtuse triangle sufficiently close to it has one of nine combinatorial types of billiard path; and any other right triangle has the property that any triangle sufficiently close to it has one of two combinatorial types of billiard path.

It seems experimentally that the obtuse isosceles triangle with small angle $\pi/2^n$ satisfies a result like Theorem 1.1. Here $n = 3, 4, 5, \ldots$. There are sporadic nonisosceles examples as well, such as the obtuse triangle with small angles $(\pi/6, \pi/12)$. These triangles are all *Veech triangles* [Masur and Tabachnikov 02], and we think that there is some connection between Theorem 1.1 and Veech triangles. We hope eventually to establish this, but at the moment it is just a thought.

Theorems 1.1 and 1.2 complement each other. Each makes the other one look more surprising. We now describe another related pair of results like this.

Theorem 1.3. *Let $\{T_n\}$ be a sequence of triangles with angles*

$$\frac{\pi}{6} + \epsilon_n, \quad \frac{\pi}{3} - \epsilon_n - \iota_n, \quad \frac{\pi}{2} + \iota_n,$$

with ϵ_n and ι_n positive. Suppose that $\lim \epsilon_n = 0$ and $\lim \iota_n/\epsilon_n = 0$. Then $\lim L_n = \infty$, where L_n is the minimal combinatorial length of a periodic billiard path on T_n.

Theorem 1.4. *Let $\{T_n\}$ be a sequence of triangles with angles*

$$\frac{\pi}{6} + \epsilon_n, \quad \frac{\pi}{3} - \epsilon_n - \iota_n, \quad \frac{\pi}{2} + \iota_n.$$

Suppose that $\lim \epsilon_n, \iota_n = 0$, and $\inf \iota_n/\epsilon_n > 0$. Then $\sup L_n < \infty$, where L_n is the minimal combinatorial length of a periodic billiard path on T_n.

We can certainly take the sequence in Theorem 1.3 to be rational. Thus, even though periodic orbits are dense on a rational triangle, Theorem 1.3 demonstrates that the *shortest* periodic billiard path on a rational triangle might be extremely long even when the geometry of the triangle is bounded.

Now we illustrate Theorem 1.2. The parameter space Δ of obtuse triangles is itself a triangle; $(x, y) \in \Delta$ represents the triangle, whose acute angles are x and y. For each word W we let $O(W) \subset \Delta$ denote the set of triangles for which W describes a periodic billiard path. We call $O(W)$ an *orbit tile*. We will cover $S_{1/400}$ with two infinite and interlocking families of orbit tiles, the Y *family* and the Z *family*. See Section 3 for definitions of these families.

Figure 1 shows a plot taken from McBilliards. We show plots of some of the Y tiles and some of the Z tiles together. The Y family alternates in color between light and lighter. The Z family alternates in color between

[1] One can play McBilliards on my website, www.math.brown.edu/~res, using a Java-enabled browser. We encourage the reader to operate this program while reading the paper, to see the mathematics in action.

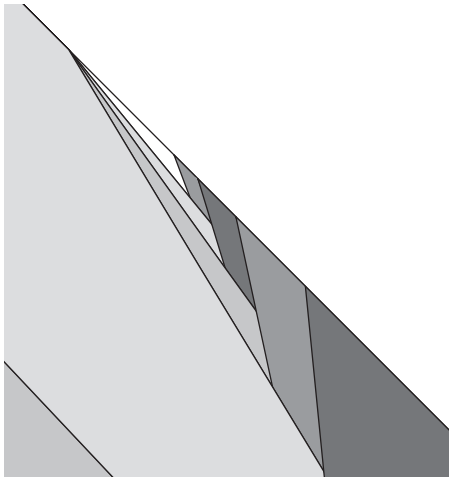

FIGURE 1.

dark and darker. The plot takes place in a neighborhood of $p_\infty = (\frac{\pi}{6}, \frac{\pi}{3})$, the point that represents T_∞. The pattern continues in the obvious way, and the "ridge" between the two families approaches p_∞ parabolically.

One thing that is not clear from the picture is that our tiles overlap each other rather than abut. (This is the usual difficulty with drawing opaque objects.) Also, the apparent straight lines in Figure 1 are actually not straight lines. This nonlinearity accounts for most of the complexity in the proof of Theorem 1.2.

Here is an overview of the paper. Our basic idea in proving Theorem 1.2 is simply to capture as much of the structure of Figure 1 as is necessary. In some places we rely on Mathematica [Wolfram 00] for symbolic manipulation, though in the most nontrivial cases we will explain mathematically how our formulas are derived. In Section 2 we will give background information. In Section 3 we will introduce the words $\{Y_k\}$ and $\{Z_k\}$. These words are responsible for the Y tiles and Z tiles discussed above. We will also compute some combinatorial objects associated with our words.

In Section 4 we will prove Theorem 1.4 using the Y family of tiles. Theorem 1.4 is a stepping stone to the proof of Theorem 1.2. Our basic idea is to use the Z tiles to fill in the gaps left over by the Y tiles. In order to get this program to work, we need a few technical estimates, and we make these in Section 5. The reader should certainly just skim these results on the first pass through the paper. In Section 6 we analyze the Z tiles and thereby finish the proof of Theorem 1.2.

Theorem 1.3 immediately implies Theorem 1.1, and the proof of Theorem 1.3 is independent from the proof of Theorems 1.2 and 1.4. The reader interested only in Theorem 1.3 can just read Section 2.1 and Sections 7 and 8. Our idea for Theorem 1.3 is to look at geometric limits of potential counterexamples to the theorem and see how they relate to the $(2, 3, 6)$ Euclidean tiling.

One key step in our proof of Theorem 1.3 is the result of Galperin–Stepin–Vorobets [Galperin et al. 91] that T_∞ does not have any *stable* periodic billiard trajectories. A periodic billiard path is stable if it works for an open set of triangles. Hooper [Hooper 06] has recently proved the instability result for all right triangles. (This was another result we discovered using McBilliards.) As we mentioned above, Theorem 1.1 is not true for other right triangles, so in light of [Hooper 06], our argument requires more than just the instability result.

The reader may wonder whether the innocent-looking Theorem 1.2 has a simpler proof. Since we don't have any better ideas currently, we can't answer this question. However, we note that Theorem 1.1 forces Theorem 1.2 to involve an infinite list of words. Also, based on months of extensive experimentation with McBilliards, we can say that our proof absolutely produces the simplest explicit list of words that work. There are other infinite families that seem also to work, but they are more complicated and we have not completely analyzed them.

2. PRELIMINARIES

2.1 Unfoldings

A *word* is a finite sequence $W = (w_1, \ldots, w_{2k})$ with no repeated indices. (We consider only even words in this paper.) Given W and a labeled triangle T we define a sequence $T_1, \ldots, T_{2k}$ of triangles by the rule that T_{j-1} and T_j are related by reflection across the w_jth edge of T_j. Here $j = 2, \ldots, 2k$. The set $U(W, T) = \{T_j\}_{j=1}^{2k}$ is known as the *unfolding* of the pair (W, T). This is a well-known construction; see [Tabachnikov 95]. Figure 2 shows $U(Y_1, T_\infty)$ and Figure 3 shows $U(Z_1, T_\infty)$. Here

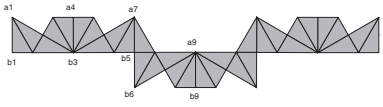

FIGURE 2.

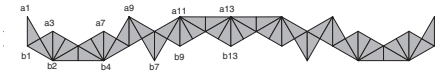

FIGURE 3.

$Y_1 = (231232\dots)$ and $Z_1 = (312323\dots)$. These words are the beginnings of the infinite families that we define in Section 3. We label the top row of vertices of $U(W,T)$ as $a_1, a_2, \dots$ from left to right. We label the bottom row of vertices of $U(W,T)$ as $b_1, b_2, \dots$, from left to right.

Let V^{-1} denote the reverse of a word V. We say that W is a *special palindrome* if $W = wVwV^{-1}$, where w is a digit and V is an odd word. In this situation, the unfolding $U(W,T)$ has a line of bilateral symmetry for any T. We also require that the first and last sides of $U(W,T)$, for any triangle T, be parallel to the line of symmetry and hence to each other. The words we consider for Theorems 1.2 and 1.4 are special palindromes; the parallel condition follows from our computations below of the so-called spine profiles. When W is a special palindrome we rotate so that the line of symmetry of $U(W,T)$ is vertical, as in Figures 2 and 3.

We call a line segment L perpendicular to the line of bilateral symmetry that joins the first and last edges of $U(W,T)$ and is contained in the interior of $U(W,T)$ a *centerline* for W. Such a line segment is horizontal. In a fairly tautological way, W describes a periodic billiard path in T iff $U(W,T)$ has a centerline. Neither $U(Y_1, T_\infty)$ nor $U(Z_1, T_\infty)$ has a centerline. However, Figures 4 and 5 show triangles T_1 and T_2 such that $U(Y_1, T_1)$ and $U(Z_1, T_2)$ have centerlines. In order to get a more detailed picture we show only the left halves of our unfoldings. The right halves are mirror images. The horizontal lines shown in Figures 4 and 5 show the boundaries of the set of centerlines. The thickened segments will be explained below.

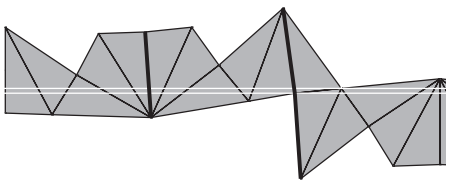

FIGURE 4.

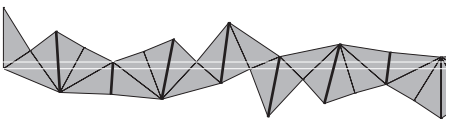

FIGURE 5.

To show that W describes a periodic billiard path for T, we have only to verify that W is a special palindrome and then check that all the a vertices in $U(W,T)$ lie above all the b vertices. We let $O(W) \subset \Delta$ denote the set of T such that $U(W,T)$ has these properties. As in the introduction, we call $O(W)$ an *orbit tile*.

We introduce the notation $v \uparrow w$ to indicate that a vertex v lies above a vertex w for all points in a certain region of Δ. In practice, the region of interest to us will be clear from the context. To show that $O(W)$ contains a certain region of parameter space we just need to show that $a_i \uparrow b_j$ for all index pairs (i,j). Given the bilateral symmetry of our tiles, we will consider only the vertices that lie on the left half of our unfoldings.

2.2 The Tilt and Spine Profiles

We say that a line segment of $U(W,T)$ is *near vertical* if the corresponding line segment is vertical for $U(W,T_\infty)$. Since we are working with special palindromes, we will consider only the near-vertical edges on the left. Also, we omit the left and center vertical edges, because these remain vertical with respect to any triangle. There are 3 near-vertical segments of $U(Y_1,T)$ and 7 near-vertical segments of $U(Z_1,T)$. See Figures 4 and 5.

Let θ'_j denote the counterclockwise angle through which the y-axis must be rotated to produce a line parallel to the jth near vertical. We take θ'_j modulo π, so that we don't have to worry about the orientations of our edges. The angle θ'_j is a function of a point $(x,y) \in \Delta$, the parameter space. Given our normalization, we have integers (M'_j, N'_j) such that

$$\theta'(x,y) = M'_i x + N'_i y.$$

We call the collection $\{(M'_j, N'_j)\}$ the *tilt profile* of the word. The tilt profiles for Y_1 and Z_1 are respectively

$$\{(-2,2),(-4,-4),(-2,-2)\}$$

and

$$\{(-2,-2),(-4,-1),(-6,0),(-8,-2),\\ (-6,0),(-4,2),(-2,1)\}.$$

We say that a triangle T is *k-normalized* if the kth side has length 1. Given a palindrome W, there is a unique minimal polygonal path, consisting of k-edges, that connects a vertex on the leftmost edge of $U(W,T)$ to a vertex on the middle edge. We call this path the *k-spine*. Figure 7 shows the 2-spine of $U(Y_1, T_\infty)$. Figure 16 shows the 1-spine of $U(Z_1, T_\infty)$. (See Section 3.)

We label the edges of the k-spine as $E_1, E_2, \dots$. Let θ_j denote the counterclockwise angle though which the y-axis must be rotated to produce a line parallel to E_j.

Again we work modulo π. Then there are integers M_j and N_j such that

$$\theta_j(x,y) = M_j x + N_j y.$$

We call the sequence $\{(M_j, N_j)\}$ the *k-spine profile* of W.

When W is a long word it makes sense to plot the k-spine profile on the integer lattice rather than list a long string of integer points. Figure 11 shows the 2-spine profiles for Y_1, Y_2, Y_3, Y_4. Figure 17 shows the 1-spine profiles for Z_1, Z_2, Z_3. (See Section 3.)

2.3 Defining Functions

Suppose that $k \in \{1,2\}$ is fixed. Let $m \le n$ be integers such that the edges $E_m, \dots, E_n$ of the k-spine exist. Let λ_m denote the left vertex of E_m and let ρ_n denote the right vertex of E_n. Let π_y denote the projection onto the yth coordinate. We define

$$f_{mn} = \pi_y(\rho_n) - \pi_y(\lambda_m).$$

This definition of course depends on whether we take $k = 1$ or $k = 2$, but in all cases the choice should be clear from the context. Figure 6 illustrates our construction for $f_{59} = \pi_y(b_6) - \pi_y(a_5)$, with respect to the word Z_1.

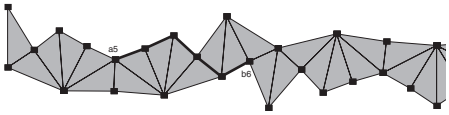

FIGURE 6.

Lemma 2.1.

$$f_{mn}(x,y) = \pm \sum_{j=m}^{n} (-1)^j \cos(M_j x + N_j y). \qquad (2\text{–}1)$$

Proof: For the purposes of derivation, let us orient E_j so that it points (roughly) from left to right. Let $\widehat{\theta}_j$ denote the counterclockwise angle through which the vector $(0,1)$ must be rotated so that it points in the same direction as E_j. This time we work modulo 2π. Let λ_j and ρ_j denote the left and right endpoints of E_j. From basic trigonometry we have $\pi_y(\lambda_j) - \pi_y(\rho_j) = \cos(\widehat{\theta}_j)$. Summing over j and using the fact that $\lambda_{j+1} = \rho_j$, we have

$$\begin{aligned} f_{mn} &= \sum_{j=m}^{n} \cos(\widehat{\theta}_j) = \pm \sum_{j=m}^{n} \cos(M_j x + N_j y + \epsilon_j \pi) \\ &= \pm \sum_{j=m}^{n} (-1)^{\epsilon_j} \cos(M_j x + N_j y), \quad \epsilon_j \in \{0,1\}. \end{aligned} \qquad (2\text{–}2)$$

To finish our derivation we just have to show that the sequence $\{\epsilon_j\}$ alternates. Suppose that $\epsilon_j = 0$. Then $\widehat{\theta}_j = M_j x + N_j y$. Let E_{j+1}^- denote the edge coinciding with E_{j+1} but having the opposite orientation. Then E_j and E_{j+1}^- both point toward $v_j = \rho_j = \lambda_{j+1}$. But then there are integers m_j and n_j such that E_{j+1}^- is obtained by rotating E_j about v_j through an angle of $m_j x + n_j y$. Here (m_j, n_j) has one of the forms $(k_j, 0)$, $(0, k_j)$, (k_j, k_j), for some $k_j \in \mathbb{Z}$. The form depends on the vertex type of v_j, and k_j is the number of triangles in the unfolding that are incident to v_j and between our two edges. So, $\widehat{\theta}_{j+1} \pm \pi$ has the form $M_{j+1} x + N_{j+1} y$. Hence $\epsilon_{j+1} = 1$. A similar argument shows that $\epsilon_{j+2} = 0$. □

Remark 2.2. The $(\pm)$ out in front of Equation (2–1) is what we call *the global sign*. It is not hard to see, for the words of interest to us in this paper, that the global sign is positive iff E_1 has negative slope.

Remark 2.3. The interested reader can see these defining functions computed automatically using the unfolding window in McBilliards.

2.4 Bounds on Partial Derivatives

We have the general bound

$$|\partial \sin(Mx + Ny)|, \quad |\partial \cos(Mx + Ny)| \le \max(|M|, |N|).$$

Here each ∂ could be either ∂_x or ∂_y. This gives us an absolute bound on and kth iterated partial derivatives:

$$|\partial^k f_{mn}| \le \sum_{j=m}^{n} \max(|M_j|^k, |N_j|^k). \qquad (2\text{–}3)$$

These bounds hold throughout the parameter space Δ.

3. THE WORDS AND THEIR PROFILES

3.1 The Y Unfoldings

In this section we introduce our words $\{Y_k\}$. To describe these words, we will draw the left halves of the unfoldings $U(Y_k, T_\infty)$ for $k = 1,2,3,4$. The obvious pattern continues. See Figures 7, 8, 9, and 10.

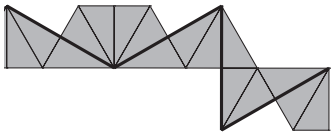

FIGURE 7.

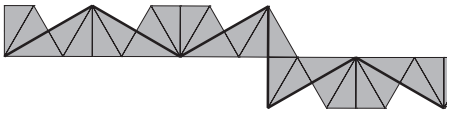

FIGURE 8.

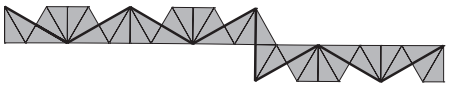

FIGURE 9.

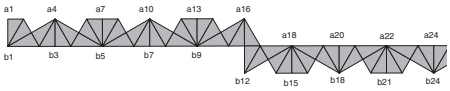

FIGURE 10.

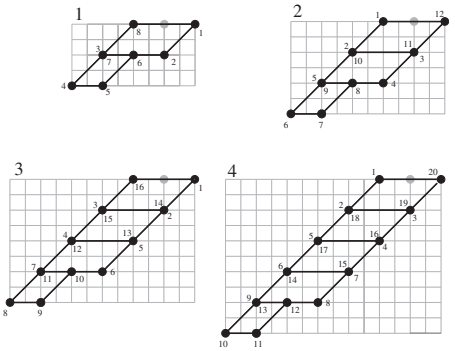

FIGURE 11.

3.2 Profiles for the Y Family

We saw in Section 2 that the tilt profile for Y_1 is $\{(-2,-2),(-4,-4),(-2,-2)\}$. We rewrite this as $\{1,2,1\}(-2,-2)$. In general, the tilt profile for Y_k is

$$\{1,2,\ldots,k,k+1,k,\ldots,2,1\}(-2,-2). \tag{3–1}$$

Figure 11 shows the 2-spine profiles for $k = 1,2,3,4$. The gray dot is the origin. The pattern continues in the obvious way: we get a growing ladder. Notice that the way in which the ladder is traced out depends (mildly) on the parity of k.

McBilliards computes these profiles automatically, and we just copied down the pattern. We point out that the very simple repetitive nature of the unfoldings allows us to easily predict the pattern from the first few instances. In [Schwartz 05a] we explain how McBilliards does these computations in general. In Section 3.5 we will explain a specialized algorithm for computing the 1-spine profiles for the Z family. This specialized algorithm does not work in general. We have chosen to focus on the Z family because this family is considerably more interesting and intricate. One can reproduce the above pictures using an algorithm similar to the one we discuss in Section 3.5.

3.3 The Z Unfoldings

Here we show the left halves of the unfoldings $U(Z_k,T_\infty)$ for $k = 1,2,3,4,5$. Equations (3–3) and (3–4) below explain the general case.

3.4 Labeled Spines for the Z Family

Let Σ_k be the 1-spine of $U(Z_k,T_\infty)$. We let $E_1,E_2,\ldots$ be the edges of Σ_k, moving from left to right. We label E_j by one of $\{+,-,0\}$ according to whether E_j lies on the upper boundary of $U(Z_k,T_\infty)$, the lower boundary, or neither boundary. We assign a second label, in $\{+,-\}$, to E_j, according to whether or not it has positive or negative slope. As one can see from Figure 16, the labeling scheme for Σ_1 is

1	2	3	4	5	6	7	8	9	10	11	12	13	14	15	16
0	+	+	+	+	+	+	0	−	0	0	−	−	−	−	−
+	+	−	−	+	+	−	−	+	+	−	−	+	+	−	−

The second label sequence for Σ_k is $+,+,-,-,+,+,-,-,\ldots$, independent of k. We can recover $U(Z_k,T_\infty)$, and hence Z_k, from the first label sequence associated with Σ_k as follows: Let $\mathcal{T}$ be the tiling of the plane by $(2,3,6)$ triangles. We draw Σ_k on $\mathcal{T}$. Let m_j be the midpoint of E_j. For each j we color in all the triangles X of $\mathcal{T}$ such that X contains a vertex with E_j and X intersects:

- $(+)$ case: the vertical downward ray starting at m_j.
- (0) case: the vertical line through m_j.
- $(-)$ case: the vertical upward ray starting at m_j.

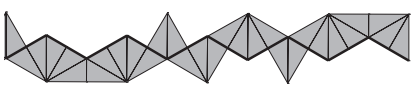

FIGURE 12.

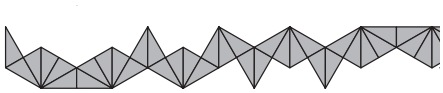

FIGURE 13.

FIGURE 14.

The union of colored triangles is $U(Z_k, T_\infty)$.

To describe the first labeling sequence in general we define

$$A = 0,+,+,+,+,+,+,0, \quad C = -,-,-,-, \tag{3–2}$$
$$B_- = -,0,0,-, \quad B_0 = 0,+,0,-, \quad B_+ = 0,+,+,0.$$

We also write $X^k = X, \ldots, X$, repeated k times. For the odd words we have

$$\Sigma_{2k-1}: \quad AB_+^{k-1}B_-^kC, \quad k = 1,2,3,4,\ldots. \tag{3–3}$$

For the even words we have

$$\Sigma_{2k}: \quad AB_+^{k-1}B_0B_-^kC, \quad k = 1,2,3,4,\ldots. \tag{3–4}$$

3.5 Computing the Z Spine Profiles

Now we explain our specialized algorithm that computes the spine profiles for the sequence above. Again, we remark that McBilliards uses a different and more general algorithm. One can use the "unfold" window in McBilliards to check that our computations here match the general computations done there.

We define the (m_j, n_j) pairs by the rule

$$(M_k, N_k) = \sum_{j=1}^{k} (m_j, n_j). \tag{3–5}$$

It turns out that $(m_1, n_1) = (0, -1)$ in all cases. For $j > 1$ the pair (m_j, n_j) associated with E_j depends on the labels of E_{j-1} and E_j. Of the 36 possibilities, 18 occur in practice. Here are 9 of them:

$$\begin{vmatrix} - & - \\ - & - \\ & 2 \\ & 2 \end{vmatrix} \begin{vmatrix} + & + \\ + & - \\ & 0 \\ & 2 \end{vmatrix} \begin{vmatrix} 0 & - \\ - & - \\ & 2 \\ & 2 \end{vmatrix} \begin{vmatrix} 0 & + \\ + & - \\ & 0 \\ & 2 \end{vmatrix} \begin{vmatrix} 0 & 0 \\ + & - \\ & 0 \\ & 2 \end{vmatrix} \begin{vmatrix} + & + \\ - & + \\ & 0 \\ & 4 \end{vmatrix} \begin{vmatrix} - & - \\ + & + \\ & 2 \\ & 2 \end{vmatrix} \begin{vmatrix} - & 0 \\ + & + \\ & 2 \\ & 2 \end{vmatrix} \begin{vmatrix} + & 0 \\ + & - \\ & 0 \\ & 2 \end{vmatrix}$$

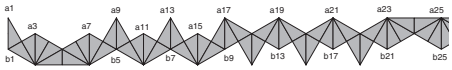

FIGURE 15.

The other 9 rules can be derived from symmetry: If we reverse all the signs of the edge labels, we also reverse the signs of the vectors. For each of the first 8 listed rules, one can find either the rule or its "negative" in Figure 16. The ninth rule appears in Figure 12.

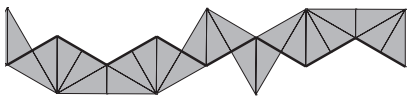

FIGURE 16.

Here we use our algorithm to obtain the 1-spine profile for Z_1. We write the (m, n) pairs below the labels:

$$\begin{array}{ccccccccccccccc} 0 & + & + & + & + & + & + & 0 & - & 0 & 0 & - & - & - & - & - \\ + & + & - & - & + & + & - & - & + & + & - & - & + & + & - & - \\ 0 & -2 & 0 & -2 & 0 & -2 & 0 & -2 & 0 & 2 & 0 & 2 & 0 & 2 & 0 & 2 \\ -1 & -2 & 2 & -2 & 4 & -2 & 2 & -2 & -2 & 2 & 2 & 2 & -2 & 2 & -4 & 2 \end{array}$$

Once we compute the 1-spine profile for Z_k we can compute the tilt profile $\{(M_j', N_j')\}$ according to the formula

$$(M_j', N_j') = \frac{1}{2}(M_{2j+2}, N_{2j+2}) + \frac{1}{2}(M_{2j+3}, N_{2j+3}),$$
$$j = 1,2,3,\ldots. \tag{3–6}$$

Figure 17 shows the 1-spine profiles for Z_1, Z_2, Z_3 in black, and the tilt profiles in gray. The pattern continues in the obvious way.

4. PROOF OF THEOREM 1.4

4.1 Proof Outline

As in the introduction, $p_\infty = (\frac{\pi}{6}, \frac{\pi}{3})$ denotes the point in $\partial\Delta$ corresponding to our favorite triangle, T_∞. We work in radians. We know that acute and right triangles have periodic billiard paths, so to prove Theorem 1.2 it suffices to consider $(x, y) \in \Delta$ with $x + y > \frac{\pi}{2}$.

Figure 18, which is a plot taken from McBilliards, shows the orbit tiles $O(Y_1)$, $O(Y_2)$, $O(Y_3)$, $O(Y_4)$, with the big tile $O(Y_1)$ partially obscuring the others. The plot takes place in a neighborhood of p_∞. First, we prove a lemma:

Lemma 4.1. *Let $S_- \subset \Delta$ denote those points (x, y) such that*

$$x + y \in \left(\frac{\pi}{2}, \frac{\pi}{2} + \frac{1}{144}\right), \quad x \in \left[\frac{\pi}{15}, \frac{\pi}{6}\right].$$

Then $S_- \subset O(Y_1)$.

After Lemma 4.1 we just have to worry about points (x, y) with $x > \frac{\pi}{6}$.

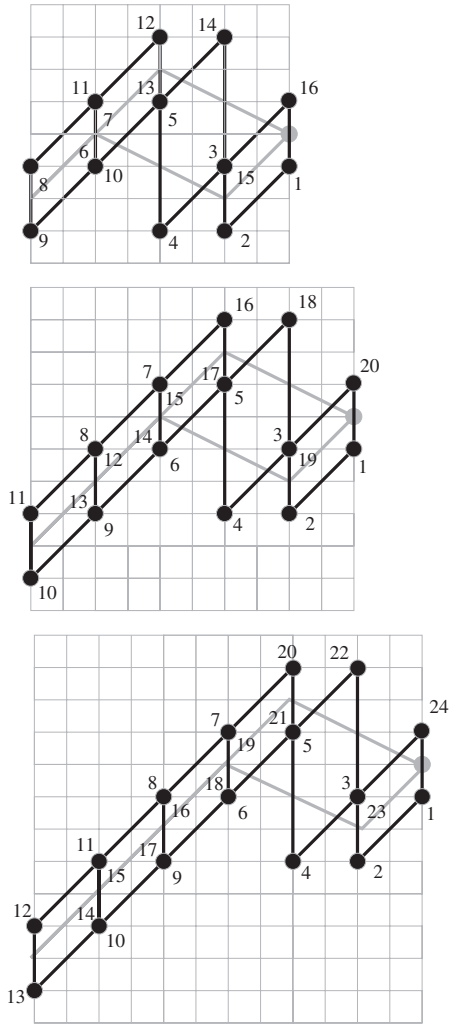

FIGURE 17.

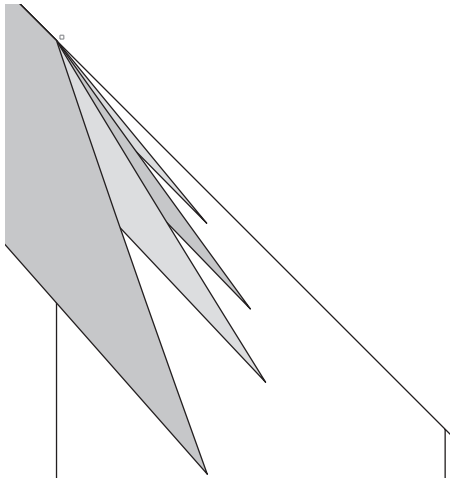

FIGURE 18.

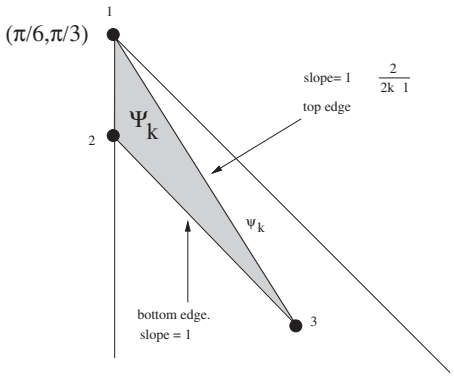

FIGURE 19.

Let $\Psi_k \subset \Delta$ be the triangular region with the following vertices:

$$1:\ p_\infty, \qquad 2:\ p_\infty + \left(0, \frac{-1}{4(k+2)^2}\right), \tag{4–1}$$
$$3:\ p_\infty + \left(\frac{2k-1}{8(k+2)^2}, \frac{-2k-1}{8(k+2)^2}\right).$$

Figure 19 shows a schematic picture of Ψ_k that retains some of the basic geometric features.

The topmost edge of Ψ_k, which we call ψ_k, has slope

$$\frac{-2k-1}{2k-1} = -1 - \frac{2}{2k-1} \in \left(-1-\frac{2}{k}, -1\right). \tag{4–2}$$

The bottom edge of Ψ_k has slope -1. For each $(x, y) \in \Psi_k$ there is some $(x, y_0) \in \partial\Delta$ such that

$$|y - y_0| \le \frac{1}{4(k+2)^2}. \tag{4–3}$$

Most of this chapter is devoted to proving the following lemma

Lemma 4.2. (Containment.) *$\Psi_k \subset O(Y_k)$ for all $k = 1, 2, 3, \ldots$.*

Our proof has six steps. At the end of the chapter we will modify our proof of the containment lemma so as to give a proof of Lemma 4.1. The containment lemma and Lemma 4.1 immediately imply Theorem 1.4. The union $\bigcup O(Y_k)$ unfortunately does not cover $S_\epsilon - S_-$ for any $\epsilon > 0$. This is why we need the Z family for Theorem 1.2.

4.2 Step 1

Lemma 4.3. *All the near-vertical lines on the left-hand side of $U(Y_k, T)$ have negative slope, provided that T corresponds to a point in Ψ_k.*

Proof: From the symmetry of the tilt profile in Equation (3–1) it suffices to take $j \le k+1$. In this case, our counterclockwise rotation angle is

$$\theta_j' = M_j' x + N_j' y = -2j(x+y) \in -2j\left(\frac{\pi}{2} - \frac{1}{4(k+2)^2}, \frac{\pi}{2}\right) \in \left(0, \frac{\pi}{20}\right) \bmod \pi. \tag{4–4}$$

This completes the proof. □

We will use Lemma 4.3 to eliminate all but 12 pairs. We will carry out Step 1 for $k = 4$. The general case follows the same pattern.

We write $a_i|a_j$ if reflection in a near-vertical line swaps a_i and a_j, and a_i lies to the left of this line of symmetry. In this case, Lemma 4.3 implies that $a_j \uparrow a_i$ throughout Ψ_4. We write $a_i|a_j|a_k$ if $a_i|a_j$ and $a_j|a_k$. Working greedily from the left we have

$$a_1|a_7|a_{13}, \quad a_2|a_6|a_8|a_{12}|a_{14}, \quad a_3|a_5|a_9|a_{11}|a_{15},$$
$$a_4|a_{10}|a_{16}, \quad a_{17}|a_{19}|a_{21}|a_{23}, \quad a_{18}|a_{22}, \quad a_{20}|a_{24}.$$

We have eliminated everything but a_1, a_2, a_3, a_4, a_{17}, a_{18}, a_{20}. Since $\overline{a_1 b_1}$ is vertical and T is obtuse, we have $a_2 \uparrow a_1$. Since the angles of T are within

$$\sup_{k \in \mathbb{N}} \frac{1}{4(k+2)^2} = \frac{1}{36} \tag{4–5}$$

of the angles of T_∞ we clearly have $a_1 \uparrow a_3$. (Here we are giving an estimate that works for all k.) Since $x < \frac{\pi}{4}$, the point a_4 lies above the line $\overline{a_3 a_5}$. This eliminates a_4. We now have eliminated everything but $a_3, a_{17}, a_{18}, a_{20}$.

Things work in the opposite direction for the b vertices. If $b_i|b_j$ we have $b_j \uparrow b_i$. This eliminates b_i (rather than b_j) from consideration. We have

$$b_1|b_5|b_9, \quad b_2|b_4|b_6|b_8|b_{10}, \quad b_3|b_7|b_{11}, \quad b_{12}|b_{18}|b_{24},$$
$$b_{13}|b_{17}|b_{19}|b_{23}, \quad b_{14}|b_{16}|b_{20}|b_{22}, \quad b_{15}|b_{21}.$$

We have eliminated everything but $b_9, b_{10}, b_{11}, b_{21}$, b_{22}, b_{23}, b_{24}. Since $\overline{a_{16} b_{10}}$ has negative slope and our triangles are obtuse, $\overline{b_{10} b_{11}}$ has positive slope. Hence $b_{11} \uparrow b_{10}$. This eliminates b_{10}. Given the estimate in Equation (4–5) and the fact that $\overline{a_{24} b_{24}}$ is always vertical, we clearly have $b_{23} \uparrow b_{21}, b_{22}, b_{23}$. We omit the easy details. We have now eliminated everything but b_9, b_{11}, b_{23}.

Table 1 shows a chart of the 12 pairs, with the a vertex indices running across the top and the b vertex indices running down the left side. The numbers in parentheses indicate the index values when $k = 4$. The numbers $2, 3, 4, 5, 6$ placed in the middle of the grid indicate the steps in which the remaining pairs are analyzed. Our chart is designed for k even. When k is odd, the value $6k-1$ must be changed to $6k-2$.

	3 (3)	$3k+5$ (17)	$3k+6$ (18)	$3k+8$ (20)
$2k+1$ (9)	6	6	6	6
$2k+3$ (11)	4	2	3	2
$6k-1$ (23)	5	5	5	5

TABLE 1.

4.3 Step 2

We will give the argument in the case $k = 4$. The general case is essentially identical. We have $b_{11}|a_{20}$. By Lemma 4.3 we have $a_{20} \uparrow b_{11}$ throughout Ψ_4. The line L through a_{17} and b_{11} bisects the fifth and sixth near verticals in the unfolding. Since these near verticals have negative slope, L has positive slope. Hence $a_{17} \uparrow b_{11}$ throughout Ψ_k.

4.4 Step 3

Let $g = \pi_y(a_{3k+6}) - \pi_y(b_{2k+3})$. Taking $m = 2k+4$ and $n = 2k+6$ in Equation (2–1), and using the fact that the cosine is an even function, we get

$$(-1)^k g(x,y) = -\cos(2kx + 2ky) + \cos((2k+2)x + 2ky) - \cos(2kx + (2k-2)y). \tag{4–6}$$

Figure 20 highlights the relevant three points on the 2-spine profile for the cases $k = 3, 4$.

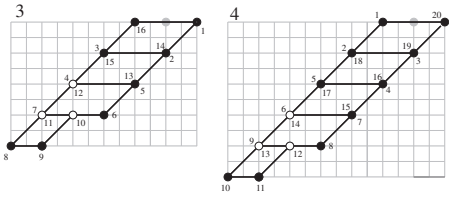

FIGURE 20.

Lemma 4.4. *$g(x,y) > 0$ when $(x,y) \in \psi_k$, the upper edge of Ψ_k.*

Proof: For ease of exposition we take k even. We can parameterize ψ_k as

$$x = \frac{\pi}{6} + t(2k-1), \quad y = \frac{\pi}{3} - t(2k+1), \quad t \in \left[0, \frac{1}{8(k+2)^2}\right]. \tag{4–7}$$

We compute that

$$g(x,y) = \cos(2t) - \cos(4kt) > 0$$

for t as in Equation (4–7). □

Lemma 4.5. *$\partial_y g(x,y) < 0$ for all $(x,y) \in \Psi_k$.*

Proof: Again we take k even for ease of exposition. We have

$$\partial_y g(x,y) = 2k\sin(\alpha) - 2k\sin(\beta) + (2k-2)\sin(\gamma), \quad (4\text{–}8)$$

where

$$\alpha = 2k(x+y), \quad \beta = \alpha + 2x, \quad \gamma = \alpha - 2y. \quad (4\text{–}9)$$

The conditions $(x,y) \in \Psi_k$ force the bounds

$$x+y \in \left(\frac{\pi}{2} - \frac{1}{4(k+2)^2}, \frac{\pi}{2}\right), \quad x \in \left(\frac{\pi}{6}, \frac{\pi}{6} + \frac{2k-1}{8(k+2)^2}\right),$$
$$pty \in \left(\frac{\pi}{3} - \frac{2k-1}{8(k+2)^2}, \frac{\pi}{3}\right).$$

This easily leads to the bounds

$$\alpha \in \left(-\frac{1}{16}, 0\right), \quad 2x \in \left(\frac{\pi}{3}, \frac{\pi}{2}\right), \quad 2y \in \left(\frac{\pi}{2}, \frac{4\pi}{3}\right).$$

Hence

$$\sin(\alpha) < 0, \quad \sin(\beta) > 0, \quad \sin(\gamma) < 0,$$

and all three terms in Equation (4–8) are negative. □

Lemmas 4.4 and 4.5 immediately imply that $g > 0$ on Ψ_k. This completes Step 3. With a view toward Lemma 4.1 we switch tracks and take $k = 1$ for a moment.

Lemma 4.6. *$g(x,y) > 0$ if $(x,y) \in \partial\Delta$ and $x < (0, \pi/6)$ and $\partial_y g(x,y) < 0$ for all $(x,y) \in S_-$.*

Proof: For $(x,y) \in \partial\Delta$ we have $y = \pi/2 - x$. Equation (4–6) simplifies to $g(x,y) = 2\cos(2x) - 1 > 0$. The positivity comes from $x \in (0, \pi/6)$. We have $\partial_y g(x,y) = 4\sin(x)\cos(3x+2y)$. This expression has the same sign as $\cos(3x+2y)$. But

$$3x + 2y = 2(x+y) + x \in \left(\pi - \frac{\pi}{2}, \pi + \frac{\pi}{2}\right)$$

for $(x,y) \in S_-$. Hence $\cos(3x+2y) < 0$. □

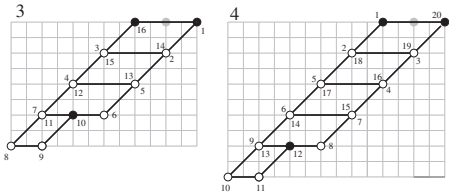

FIGURE 21.

4.5 Step 4

We define $g(x,y) = f_{2,2k+3} = \pi_y(b_{2k+3}) - \pi_y(a_3)$. Figure 21 shows the relevant points (in white) on the 2-spine profiles, in the cases $k = 3, 4$. Notice that there is a symmetry to the white points that is broken only in the last row.

We have $g = g_1 + g_2$, where

$$g_1 = \sum_{j=1}^{k} \cos((-2j-2)x - 2jy)) - \cos((-2j+2)x - 2jy),$$
$$g_2 = \cos((-2k+2)x - 2ky) - \cos(-2kx - 2ky).$$

When $y = \pi/2 - x$ each summand in the equation for g_1 is zero, and hence $g_1 = 0$. On the other hand, $g_2 = -2\sin^2(x)$. Hence

$$g|_{\partial\Delta} = -2\sin^2(x).$$

Equation (2–3) gives us

$$|\partial_g y| \le 2\sum_{j=1}^{k+1} 2j = 2(k+1)(k+2). \quad (4\text{–}10)$$

Let y_0 be such that $(x, y_0) \in \partial\Delta$. Integrating Equation (4–10) and using Equation (4–3) gives uss

$$g(x,y) < -2\sin^2(x) + 2(k+1)(k+2) \times \frac{1}{4(k+2)^2}$$
$$< -\frac{1}{2} + \frac{1}{2} = 0.$$

Here we are using the fact that $x \in (\frac{\pi}{6}, \frac{\pi}{2})$ so that $-2\sin^2(x) < -\frac{1}{2}$.

4.6 Step 5

In this section we will show that $b_{2k+3} \uparrow b_{6k-1}$ throughout Ψ_k. This will eliminate b_{6k-1}. Define $g(x,y) = f_{2k+4,4k+3} = \pi_y(b_{6k-1}) - \pi_y(b_{2k+3})$. Essentially the same proof as in Step 4 shows that $g(x,y) = -2\sin^2(x)$ for $(x,y) \in \partial\Delta$. Equation (4–10) remains true for our function g here. Actually, we get the stronger bound $|\partial_y g| \le 2k(k+1)$. The rest of the proof is as in Step 4.

4.7 Step 6

We will do this step for $k = 4$. The general case is the same. Let I denote rotation by π through the point b_{11}. If T is an obtuse triangle then the polygonal path $b_9 b_{11} a_{18}$ bends down. Hence $I(a_{18}) \uparrow b_9$. We already know that $a_{18} \uparrow b_{11}$ throughout Ψ_4. Hence $b_{11} \uparrow I(a_{18})$. Hence $b_{11} \uparrow I(a_{18}) \uparrow b_9$. This eliminates b_9 from consideration.

4.8 Proof of Lemma 4.1

The proof of Lemma 4.1 follows the same steps as the proof of the containment lemma. Steps 1, 2, and 6 go through word for word. Step 3 goes through word for word, with Lemma 4.6 replacing Lemma 4.4.

For Step 4 let $(x, y) \in S_-$. Then let (x, y_0) be the corresponding point in $\partial\Delta$. We have

$$g(x, y_0) \le -2\sin^2\left(\frac{\pi}{15}\right) < -\frac{1}{12}. \tag{4–11}$$

On the other hand, throughout Δ we have

$$|\partial_y g| \le 2(1+1)(1+2) = 12.$$

Finally,

$$|y - y_0| < \frac{1}{144},$$

and hence

$$g(x, y) < g(x, y_0) + 12 \times \frac{1}{144} < \frac{-1}{12} + \frac{1}{12} = 0.$$

In short, $g(x, y) < 0$. Step 5 works the same way as Step 4. This completes the proof of Lemma 4.1.

5. SOME TECHNICAL ESTIMATES

Here we prove some technical estimates that help us analyze how the Y tiles and Z tiles interact.

Let $v_k = (x_k, \frac{\pi}{2} - x_k) = p_\infty + (\theta_k, -\theta_k)$, where

$$-\frac{\sin(5x_k)}{\sin(7x_k)} = \frac{\cos(5\theta_k) - \sqrt{3}\sin(5\theta_k)}{\cos(7\theta) + \sqrt{3}\sin(7\theta)} = \frac{k}{k+1}, \quad k \in \mathbb{N}. \tag{5–1}$$

Here θ_k is the least positive solution and $x_k = \frac{\pi}{6} + \theta_k$. It turns out $\partial\Delta \cap \overline{O(Z_k)}$ is a segment bounded by the points v_k and v_{k+1}.

Lemma 5.1. *$\theta_k < 1/(20k)$ for $k = 1, 2, \ldots$. Also, $\theta_1 > \theta_2 > \theta_3, \ldots$.*

Proof: Let $\phi(\theta)$ denote the middle expression of Equation (5–1). We compute that $\phi(0) = 1$ and $\phi(\pi/30) = 0$. Let $I = [0, \pi/30]$. We compute that $\phi''(\theta) = 4P(\theta)/(Q(\theta)^3)$, where $Q(\theta) = \cos(7\theta) + \sqrt{3}\sin(7\theta) > 0$ and

$$P(\theta) = 61[\cos(5\theta) - \sqrt{3}\sin(5\theta)] + 72\cos(9\theta) - \cos(19\theta) - \sqrt{3}\sin(19\theta).$$

We have $5\theta \in [0, \pi/6]$, which makes the bracketed term nonnegative. Since $9\theta \in [0, \pi/3]$, the rest of the sum for $P(\theta)$ is positive. Hence $\phi'' > 0$ on I.

We compute that $\phi'(\pi/30) < 0$. Since $\phi'' > 0$ on I we conclude that $\phi' < 0$ on I. Hence ϕ decreases monotonically from 1 to 0 on I. In particular, a least positive solution $\theta_k \in I$ exists to Equation (5–1) for $k = 1, 2, 3, \ldots$. Since the $k/(k+1)$ are increasing, the sequence $\{\theta_k\}$ is monotone decreasing.

We compute that $\phi'(1/800) < -20$. Hence $\phi'(t) < -20$ for $t \in [0, 1/800]$. We compute that $\phi(1/800) < 40/41$. Hence $\theta_k \in [0, 1/800]$ for $k \ge 40$. So

$$\frac{1}{k} > \frac{1}{k+1} = 1 - \frac{k}{k+1} = \phi(0) - \phi(\theta_k) = \int_0^{\theta_k} (-\phi'(s))ds > 20\theta_k.$$

Rearranging this equation gives us our estimate for $k \ge 40$. We then show by direct computation in Mathematica that

$$\phi\left(\frac{1}{20k}\right) < \frac{k}{k+1}, \quad k = 1, \ldots, 40.$$

This result, and monotonicity, takes care of the first few cases. □

Let Λ_k denote the line of slope $-1 - \frac{4}{k}$ through v_k. It turns out that Λ_k is an estimator for the edge of $O(Z_k)$ emanating from v_k. Recall that ψ_k is the top edge of Ψ_k.

Lemma 5.2. *For $k \ge 8$ the point $X_k = \psi_k \cap \Lambda_k$ lies to the left of the point $\zeta_k = \psi_k \cap \Psi_{k+1}$.*

Proof: We compute that

$$\zeta_k = p_\infty + \left(\frac{2k-1}{8(k+3)^2}, \frac{-2k-1}{8(k+3)^2}\right).$$

We can simplify our problem by subtracting off p_∞ from all our quantities. Looking at Equation (4–1) we see that it suffices to prove that the line of slope $-1 - \frac{4}{k}$ through $(\theta_k, -\theta_k)$ intersects the segment σ whose endpoints are

$$(0, 0), \quad \left(\frac{2k-1}{8(3+k)^2}, \frac{-2k-1}{8(k+3)^2}\right).$$

Since $\theta_k < 1/(20k)$ it suffices to prove that the line Λ'_k of slope $-1-\frac{4}{k}$ through $(\frac{1}{20k}, -\frac{1}{20k})$ intersects σ. We compute this intersection point to be

$$A'_k = \left(\frac{2k-1}{10k(3k-2)}, \frac{-2k-1}{10k(3k-2)} \right) \tag{5–2}$$

We see easily that $10k(3k-2) > 8(k+3)^2$ for $k \geq 8$. Hence our intersection point lies on σ for such values of k. □

Let R_k be the region bounded by ψ_k, by $\partial\Delta$, and by the line of slope 1 through $X_k = \psi_k \cap \Lambda_k$. Then R_k is the shaded region shown on the right-hand side of Figure 22. It turns out that we shall not need the whole tile $O(Z_k)$ but only the intersection $\Omega_k = O(Z_k) \cap R_k$.

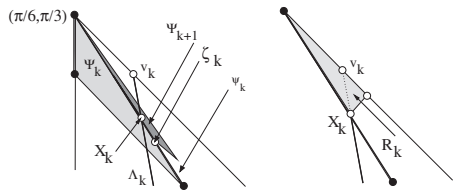

FIGURE 22.

Recall that S_ϵ denotes the set of obtuse triangles T such that the jth angle of T is within ϵ radians of $j\pi/6$ for $j = 1, 2, 3$.

Lemma 5.3. *Let $k \geq 8$ and let $p_2 \in R_k$. The point $p_1 \in \partial\Delta$ closest to p_2 lies within $1/(18k^2)$ of p_2. Furthermore, $R_k \subset S_{1/(12k)}$.*

Proof: The line Λ'_k discussed above is parallel to Λ_k and lies to the right of Λ_k. The intersection $X'_k = \Lambda'_k \cap \psi_k = p_\infty + A'_k$ lies to the right of X_k. Here A'_k is as in Equation (5–2), namely,

$$A'_k = \left(\frac{2k-1}{10k(3k-2)}, \frac{-2k-1}{10k(3k-2)} \right).$$

We have $R_k \subset R'_k$, where R'_k is the triangle bounded by $\partial\Delta$, by ψ_k, and by the line of slope 1 through X'_k. The vertices of R'_k are

$$\mathbf{1}.\ p_\infty, \quad \mathbf{2}.\ p_\infty + A'_k \quad \mathbf{3}.\ p_\infty + A'_k - B'_k,$$

where

$$B'_k = \left(\frac{1}{10k(3k-2)}, \frac{1}{10k(3k-2)} \right).$$

We remind the reader that $p_\infty = (\frac{\pi}{6}, \frac{\pi}{3})$.

Vertex 3 is the point of $\partial\Delta$ closest to vertex 2, and this distance is

$$\frac{2}{\sqrt{2}(10k(3k-2))} < \frac{1}{18k^2}.$$

Moreover, vertex 2 is the point of R'_k farthest from $\partial\Delta$. This proves our first claim.

Let V_{ij} denote the jth coordinate of vertex i. Let $V_{i3} = \pi - V_{i1} - V_{i2}$. For our second claim we need to verify

$$\left| V_{ij} - \frac{j\pi}{6} \right| \leq \frac{1}{12k}, \quad i = 2, 3, \quad j = 1, 2, 3.$$

All these bounds are easily checked and come down to the fact that

$$\frac{2k+1}{10k(3k-2)} < \frac{1}{12k}$$

as long as $k \geq 8$. □

6. PROOF OF THEOREM 1.2

6.1 Proof Outline

Let R_k be as in Lemma 5.3. The sets

$$\Omega_k = O(Z_k) \cap R_k, \quad k = 8, 9, 10, \ldots, \tag{6–1}$$

are the key to proving Theorem 1.2. These sets are approximately the same as the dark regions shown in Figure 1. We will prove the following statements:

- Ω_k is an embedded piecewise analytic quadrilateral.
- The top edge of Ω_k is the line segment bounded by v_k and v_{k+1}.
- The bottom edge of Ω_k is a line segment on ψ_k that lies to the left of A_k.
- The left and right edges of Ω_k intersect ψ_k and ψ_{k+1} once each.
- Below their common vertex v_{k+1}, the right edge of Ω_{k+1} lies to the right of the left edge of Ω_k.
- The left edge of Ω_{k+1} is disjoint from the left edge of Ω_k.

The left-hand side of Figure 23 shows a topologically accurate picture of the situation.

Given Lemma 5.2 and the intersection properties just discussed, we see that the union

$$\bigcup_{k=8}^{\infty} (\Omega_k \cup \Psi_k) \tag{6–2}$$

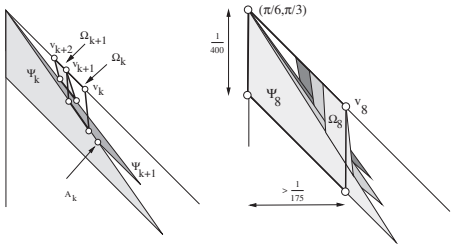

FIGURE 23.

is topologically conjugate to the picture suggested by the right-hand side of Figure 23 and therefore covers the parallelogram $P \subset \Delta$ bounded by the vertical lines through p_∞ and v_8, by $\partial\Delta$, and by the bottom edge of Ψ_8.

The width and height of P are respectively at least $1/(21 \times 8) = 1/168$ and $1/(4 \times 10^2) = 1/400$. Since P is covered by the set in Equation (6–2), which is in turn covered by orbit tiles, P is covered by orbit tiles. This result, together with Lemma 4.1, establishes Theorem 1.2. To complete our proof, we just have to establish the six claims above. Here is an overview of how we will do this.

1. We will show that $a_i \uparrow b_j$ for all (i,j) with nine exceptions:

$$i \in \{5, 2k+6, 3k+7\}, \quad j \in \{1, k+5, 3k+8\}.$$

2. We will show that $a_{2k+6} \uparrow b_{k+5}$. This pair is responsible for the top edge of Ω_k, the edge in $\partial\Delta$. Likewise we will show that $a_5 \uparrow b_1$. This pair is responsible for an edge of $O(Z_k)$ that does not intersect R_k.

3. We analyze the defining function g_{k0} for the pair (b_1, a_{2k+6}). We will verify that $\nabla g_{k0} \neq 0$, that $g_{k0}(v_k) = 0$, and that the slope of the zero set ρ_k lies everywhere in $(-\infty, -1 - \frac{4}{k})$. It turns out that ρ_k is the right edge of Ω_k. Our slope estimate guarantees that ρ_k intersects ψ_k and ψ_{k+1} exactly once. Our slope estimate combines with Lemma 5.2 to show that $\rho_k \cap \psi_k$ lies to the left of A_k.

4. We analyze the defining function g_{k1} for the pair (a_5, b_{k+5}). We will verify all the same claims as in the previous step, with $k+1$ in place of k. The zero set λ_k turns out to be the left edge of Ω_k.

5. By considering $g_{k+1,0} - g_{k1}$ we show that ρ_{k+1} lies to the right of λ_k.

6. By considering $g_{k0} - g_{k1}$ we show that λ_k and ρ_k do not cross. Let Ω_k' denote the piecewise analytic quadrilateral bounded by $\partial\Delta$ and ρ_k and λ_k and ψ_k.

7. We show that $b_{k+5} \uparrow b_{3k+8}$ and that $a_{2k+6} \uparrow a_{3k+7}$ throughout Ω_k'. This step eliminates the last two vertex pairs, and shows that $\Omega_k' = \Omega_k$.

6.2 Step 1

We write $(x,y) = p_\infty + (\delta_x, \delta_y)$. Let R_k be as in Lemma 5.3. For $(x,y) \in R_k$ we have three conditions

$$\mathbf{1}.\ \delta_x \in \left(0, \frac{1}{12k}\right), \quad \mathbf{2}.\ \frac{-\delta_x}{\delta_y} \in \left(\frac{k}{k+2}, 1\right), \quad \mathbf{3}.\ \delta_x + \delta_y < 0. \tag{6–3}$$

Condition 1 is from Lemma 5.3 and Condition 2 is from Equation (4–2).

We will illustrate Step 1 for $k = 5$. This step uses only Step 2 of Equation (6–3) and thus works for $k \geq 5$. (Actually, it works for all k.)

Lemma 6.1. *All the near-vertical lines on the left-hand side of $U(Z_k, T)$, except the first, have positive slope when T corresponds to a point in R_k.*

Proof: Figure 24 shows the tilt profile for Z_5, and its relation to the vector (δ_x, δ_y). The white ray L is parallel to $(-\delta_y, \delta_x)$ and perpendicular to (δ_x, δ_y). The gray cone is bounded by lines of slope $k/(k+3)$ and 1.

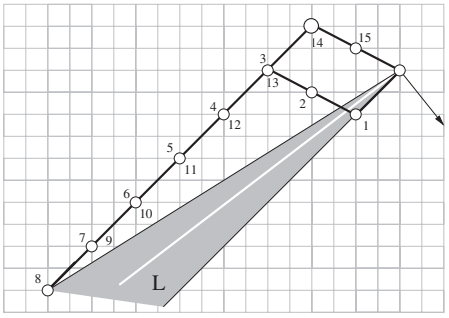

FIGURE 24.

From Condition 2 of Equation (6–3) we see that L lies in the interior of this gray cone and hence separates $(M_1', N_1') = (-2, -2)$ from (N_j', M_j') for $j = 2, \ldots, 15$. We compute modulo π that $\theta_1' = -\pi - 2(\delta_x + \delta_y) \in (0, \pi/2)$. Hence the first near-vertical has negative slope. We compute $\theta_{14}' = -4x + 2y = -4\delta_x + 2\delta_y$. It follows from Equation (6–3) that $|-4\delta_x + 2\delta_y| < \frac{\pi}{3}$. We know that $\theta_{14}' < 0$ because (M_{14}', N_{14}') lies to the left of the white line. Hence $\theta_{14}' \in (-\pi/3, 0)$. By convexity, (M_{14}', N_{14}') lies furthest from the white line. Hence, the same estimate holds for θ_j' for all $j = 2, \ldots, 15$. □

Now we are ready to make a tilting argument like the one we made in Step 1 of Section 4. We write $a_i | a_j$

if a_i lies to the left of a_j and a_i and a_j are swapped by reflection in a near-vertical that is not the first near-vertical. In this case we have $a_i \uparrow a_j$. Working greedily from the left we have

$$a_1|a_9|a_{13}|a_{17}|a_{19}|a_{21}|a_{23}|a_{25}, \quad a_2|a_8|a_{10}|a_{12}|a_{14}|a_{16},$$
$$a_3|a_7|a_{11}|a_{15}, \quad a_4|a_6|a_8, \quad a_5, \quad a_{18}|a_{20}|a_{22}.$$

We have eliminated everything but a_5, a_{15}, a_{16}, a_{22}, a_{24}, a_{25}. Note that a_{15} lies above the line $\overline{a_{14}a_{16}}$. This eliminates a_{15}. Since $x > \pi/6$ the line $\overline{a_{24}a_{25}}$ has negative slope. Hence $a_{24} \uparrow a_{25}$. This eliminates a_{24}. For $(x, y) \in S_{1/12k}$ and k moderately large—the condition $k \geq 5$ works easily—we have $a_{25} \uparrow a_{22}$. We omit the routine calculation, noting that the result becomes increasingly obvious as k increases. We have now eliminated everything but a_5, a_{16}, a_{22}.

For the B vertices we have

$$b_1|b_5|b_7|b_9|b_{13}|b_{17}|b_{21}|b_{25}, \quad b_2|b_4|b_6|b_8, \quad b_3,$$
$$b_{10}|b_{12}|b_{14}|b_{16}|b_{18}|b_{20}|b_{22}|b_{24}, \quad b_{11}|b_{15}|b_{19},$$
$$b_{13}|b_{17}|b_{21}|b_{25}, \quad b_{23}.$$

This eliminates everything but $b_1, b_2, b_3, b_{10}, b_{11}, b_{13}, b_{23}$. Given that the angles of our triangle are within $1/12k = 1/60$ radians of the angles of T_∞, the points b_2, b_3, b_4 lie below the line $\overline{b_1 b_5}$. We omit the details of this routine but tedious computation. Again, we remark that this statement becomes more obvious as k increases. Since $b_1 \uparrow b_5$ we also have $b_1 \uparrow b_2, b_3$. This eliminates b_2 and b_3. By convexity, b_{11} lies below the line $\overline{b_{10}b_{12}}$. This eliminates b_{11}. Likewise, b_{13} lies below the line $\overline{b_{12}b_{14}}$. This eliminates b_{13}. We have now eliminated everything but b_1, b_{10}, b_{23}.

6.3 Step 2

Throughout R_5: $b_1|a_5$ and the first near-vertical has negative slope. Hence $a_5 \uparrow b_1$. Likewise, $a_{16}|b_{10}$ and the eighth near-vertical has positive slope. Hence $a_{16} \uparrow b_{10}$. The proof here depends only on the sign of two of the slopes on the tilt profile and works the same for general k.

6.4 Step 3

We illustrate our equations with the case $k = 5$ but take $k \geq 8$ when it comes time to make estimates. When $k = 5$ our defining function is $g = \pi_y(a_{16}) - \pi_y(b_1)$. Taking $m = 1$ and $n = 15$ in Equation (2–1) we get the following formula for $g = g_{50}$:

$$\begin{aligned} &\cos(0x - 1y) - \cos(-2x - 3y) + \cos(-2x - y) \\ &- \cos(-4x - 3y) + \cos(-4x + y) - \cos(-6x - y) \\ &+ \cos(-6x + y) - \cos(-8x - y) + \cos(-8x - 3y) \\ &- \cos(-10x - 5y) + \cos(-10x - 3y) - \cos(-12x - 5y) \\ &+ \cos(-12x - 7y) - \cos(-14x - 9y) + \cos(-14x - 7y). \end{aligned} \tag{6–4}$$

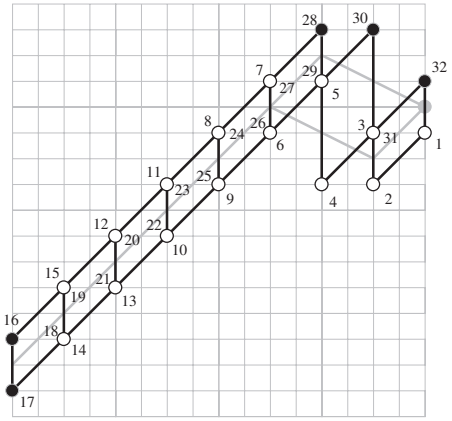

FIGURE 25.

Equation (6–4) can be read off from the 1-spine profile for Z_5, shown in Figure 25. We just find the coordinates of the white dots.

We first figure out where g vanishes along $\partial\Delta$. When we set $y = \pi/2 - x$, Equation (6–4) massively simplifies, because the only possibilities for $M_j - N_j$ are $\{1, -1, -5, -7\}$. Keeping track of the number of each kind of term, we get

$$\gamma(x) := g\left(x, \frac{\pi}{2} - x\right) = 6\sin(5x) + 5\sin(7x).$$

Setting $\gamma(x) = 0$ and writing $x = \pi/6 + \theta$ we get precisely Equation (5–1). Hence $g(v_5) = 0$. The general case works exactly the same way, with k in place of 5 and $k + 1$ in place of 6.

Now we study the gradient along the boundary. We define

$$G_x(x) = \partial_x g\left(\left(x, \frac{\pi}{2} - x\right)\right), \quad G_y(x) = \partial_x g\left(\left(x, \frac{\pi}{2} - x\right)\right).$$

Lemma 6.2.

$$\frac{G_x}{\cos(x)} = (2k^2 + 10k)\cos(6x) + 8\cos(4x) - 8\cos(2x) - 4 \tag{6–5}$$

and

$$\begin{aligned} \frac{G_y}{\cos(x)} &= (2k^2 - 4k)\cos(6x) + (4k - 2)\cos(4x) \\ &\quad - (4k - 2)\cos(2x) + (2k - 9). \end{aligned} \tag{6–6}$$

Proof: We will proceed by induction. We check explicitly that the formula holds for $k = 5, 6$. We set

$$h_k(x) = g_{k,0}\left(x, \frac{\pi}{2} - x\right) - g_{k-2,0}\left(x, \frac{\pi}{2} - x\right).$$

Looking at our spine profiles, or else at the pattern implied by Equation (6–4), we see that

$$\begin{aligned} h_k(x) = &-\cos((2k+2)x + (2k-5)y) \\ &+\cos((2k+2)x + (2k-3)y) \\ &+\cos((2k+4)x + (2k-3)y) \\ &-\cos((2k+4)x + (2k-1)y). \end{aligned}$$

After some simplification we get

$$\begin{aligned} \frac{\partial_x h_k}{\cos(x)} &= (8k+12)\cos(6x), \\ \frac{\partial_y h_k}{\cos(x)} &= (8k-16)\cos(6x) + 8\cos(4x) - 8\cos(2x) + 4. \end{aligned}$$

Equations (6–5) and (6–6) for general k now follow by induction. □

Lemma 6.3. *For $(x, y) \in \partial\Delta \cap R_k$ we have*

$$\frac{G_x(x)}{\cos(x)} < (2k^2 + 10k)\cos(6x) < 0. \tag{6–7}$$

Proof: Given that

$$x \in \left(\frac{\pi}{6}, \frac{\pi}{6} + \frac{1}{12k}\right), \tag{6–8}$$

all the individual terms in Equation (6–5) are negative. □

Lemma 6.4. *For $(x, y) \in \partial\Delta \cap R_k$ we have*

$$0 > \frac{G_y}{\cos(x)} > (2k^2 - 2k + 8)\cos(6x) \tag{6–9}$$

as long as $k \geq 8$.

Proof: After some trial and error we found that Equation (6–6) yields

$$\frac{G_y}{\cos(x)} = (2k^2 - 2k + 8)\cos(6x) + A + B + C, \tag{6–10}$$

where

$$\begin{aligned} A &= (4k-2)(-\cos(6x) + \cos(4x) - \cos(2x)), \\ B &= 2k(1 + \cos(6x)), \quad C = -10\cos(6x) - 9. \end{aligned}$$

Considering A as a function of x we have

$$\begin{aligned} &A(\pi/6) = 0, \\ &A'(\pi/6) = -(4k-2)\sqrt{3}, \\ &|A''(x)| \leq 54(4k-2) \quad \text{for all } x. \end{aligned}$$

If follows from Taylor's theorem with remainder that

$$\begin{aligned} |A| &\leq \frac{\sqrt{3}(4k-2)}{12k} + \frac{1}{2} \times \left(\frac{1}{12k}\right)^2 \times 54(4k-2) \\ &< \frac{\sqrt{3}}{3} + \frac{1}{100} < \frac{3}{5}. \end{aligned}$$

This certainly holds when $k \geq 8$. Also, $B > 0$ and $C > \frac{3}{5}$ when x is as in Equation (6–8) and $k \geq 8$. Therefore $A+B+C > 0$. Also, the first term on the right-hand side of Equation (6–10) is much more negative than $A+B+C$ is positive. This gives us Equation (6–9). □

Lemma 6.5. *Let $p_2 \in R_k$ be any point. Let $p_1 \in \partial\Delta \cap R_k$ be the point closest to p_2. Then $|\partial_u g(p_1) - \partial_u g(p_2)| \leq k$ as long as $k \geq 8$. Here $u = x, y$.*

Proof: The pattern in Equation (6–4) generalizes in an obvious way and we get from Equation (2–3) that

$$\begin{aligned} |\partial^2 g| &\leq 2\sum_{j=1}^{2k+4} j^2 < 2\int_0^{2k+5} t^2\, dt \\ &= \frac{2}{3}(2k+5)^3 < 9\sqrt{2}k^3. \end{aligned} \tag{6–11}$$

The distance between p_1 and p_2 is at most $1/(18k^2)$ by Lemma 5.3. Since $\partial\Delta$ (we mean the boundary of Δ) has slope -1 we can apply the Pythagorean theorem to conclude that each coordinate of p_1 is within $1/(18\sqrt{2}k^2)$. Integrating Equation (6–11), first in the x direction and then in the y direction, we get

$$|\partial_u g(p_1) - \partial_u g(p_2)| \leq 2 \times 9\sqrt{2}k^3 \times \frac{1}{18\sqrt{2}k^2} = k.$$

□

For x in Equation (6–8) and $k \geq 8$ we have

$$\cos(x)\cos(6x) < \cos\left(\frac{\pi}{6} + \frac{1}{96}\right)\cos\left(\pi + \frac{1}{16}\right) < -\frac{5}{6}. \tag{6–12}$$

Equations (6–7) and (6–9) now give

$$\begin{aligned} &G_x < -\lambda(x)(2k^2 + 10k), \quad G_y > -\lambda(x)(2k^2 - 2k + 8), \\ &\lambda(x) > \frac{5}{6}. \end{aligned} \tag{6–13}$$

Here x is the first coordinate of the point p_1 in Lemma 6.5.

Equation (6–13) combines with Lemma 6.5 to show that

$$\begin{aligned}\partial_x g(p_2) &< -\lambda(x)(2k^2+10k)+k \\ &= -\lambda(x)\left(2k^2+10k-\frac{k}{\lambda(x)}\right) \\ &< -\lambda(x)\left(2k^2+10k-\frac{6}{5}k\right) = -\lambda(x)\left(2k^2+\frac{44k}{5}\right)\end{aligned}$$

Similarly,

$$\begin{aligned}0 > \partial_y g(p_2) &> -\lambda(x)(2k^2-2k+8)+k \\ &= -\lambda(x)\left(2k^2-2k+\frac{k}{\lambda(x)}\right) \\ &> -\lambda(x)\left(2k^2-2k+\frac{6}{5}k+8\right) \\ &= -\lambda(x)\left(2k^2-\frac{4k}{5}+8\right).\end{aligned}$$

Therefore

$$-\frac{\partial_x g(p_2)}{\partial_y g(p_2)} < -\frac{2k^2+\frac{44k}{5}}{2k^2-\frac{4k}{5}+8} < -1-\frac{4}{k}. \qquad (6\text{–}14)$$

The last inequality holds for $k \geq 8$, and is established using a bit of calculus. The quantity on the left in Equation (6–14) is the slope of the level set through p_2. In particular, $\nabla g \neq 0$ in R_k. This finishes our analysis of the defining function g_{k0}. We have established all our claims.

6.5 Step 4

In this section we deal with g_{k1}. When $k = 5$ we have $g = \pi_y(a_5) - \pi_y(b_{10})$. Taking $m = 5$ and $n = 17$ in Equation (2–1) we get

$$\begin{aligned}&+\cos(-4x+y)-\cos(-6x-y)+\cos(-6x+y) \\ &-\cos(-8x-y)+\cos(-8x-3y)-\cos(-10x-5y) \\ &+\cos(-10x-3y)-\cos(-12x-5y)+\cos(-12x-7y) \\ &-\cos(-14x-9y)+\cos(-14x-7y)-\cos(-16x-9y) \\ &+\cos(-16x-11y).\end{aligned}$$

We compute

$$\begin{aligned}g_{k1}-g_{k+1,0} = &-\cos(y)-\cos(2x+y)+\cos(2x+3y) \\ &+\cos(4x+3y). \qquad (6\text{–}15)\end{aligned}$$

This holds independent of k for the following reason: As k increases, the same terms are added to both functions. When we set $y = \pi/2 - x$ the expression on the right-hand side of Equation (6–15) vanishes. Hence our two functions agree on $\partial\Delta$. In particular, $g_{k1}(v_{k+1}) = 0$.

Differentiating Equation (6–15), we find that

$$\frac{\partial g_{k1}(x, \frac{\pi}{2}-x)}{\cos(x)} = \frac{\partial g_{k+1,0}(x, \frac{\pi}{2}-x)}{\cos(x)} + 8.$$

The answer is the same for both partial derivatives. The same steps as those taken (for $k+1$) in Step 3 yield

$$-\frac{\partial_x g(p_2)}{\partial_y g(p_2)} < -\frac{2(k+1)^2+\frac{44(k+1)}{5}+8}{2(k+1)^2-\frac{4(k+1)}{5}+16} < -1-\frac{4}{k+1}. \qquad (6\text{–}16)$$

The last inequality holds as long as $k \geq 8$.

6.6 Step 5

Let us reconsider $h_k = g_{k+1,0} - g_{k1}$. We already know that $h \equiv 0$ on $\partial\Delta$. The right-hand side of Equation (6–15) is the same as $-8\cos(x)\cos(x+y)\sin^2(x+y)$. Given that $(x, y) \in S_{1/12k}$ we have $\cos(x+y) < 0$ and $\cos(x) > 0$. Hence $h(x, y) > 0$ for all $(x, y) \in R_k$. Thus the level set ρ_{k+1} of $g_{k+1,0}$ cannot cross the level set λ_k of g_{k1} in the interior of R_k. (In Step 4 we saw that these level sets have the common vertex $v_{k+1} \in \partial\Delta$.)

Note that both $g_{k+1,0}$ and g_{k1} are positive at p_∞. As we move along R_k parallel to $\partial\Delta$, but slightly below $\partial\Delta$, both functions eventually decrease to 0. Since $h > 0$ it must happen that g_{k1} becomes 0 before $g_{k+1,0}$ does. Hence ρ_{k+1} lies to the right of λ_k.

6.7 Step 6

Let $h = g_{k0} - g_{k1}$. We compute

$$\begin{aligned}h(x,y) = &\cos(y)+\cos(2x+y)-\cos(2x+3y) \\ &-\cos(4x+3y)+\cos((2k+6)x+(2k-1)y) \\ &-\cos((2k+8)x+(2k+1)y).\end{aligned}$$

To show that λ_k lies to the left of ρ_k it suffices to show that $h > 0$ in R_k.

Setting $y = \pi/2 - x$ gives $h = -\sin(7x) - \sin(5x)$ independent of k. For x as in Equation (6–8) we have $h > 0$. To finish our proof, it suffices to show that $\partial_y(h) > 0$ in R_k. We will make the same kind of analysis we made in Section 6.4. Let $H_y = \partial_y h(x, \pi/2 - x)$. We find that

$$\frac{H_y}{2\cos(x)} = -(2k-1)\cos(6x) - 2\cos(4x) + 2\cos(2x) - 5. \qquad (6\text{–}17)$$

The first three terms on the right-hand side are positive. Hence, from Equation (6–12) we get

$$H_y > \frac{5}{3}(2k-1) - 10.$$

From Equation (2–3) we get

$$\begin{aligned}|\partial^2 h| &\le 1 + 2^2 + 3^2 + 4^2 + (2k+6)^2 + (2k+8)^2 \\ &= 130 + 56k + 8k^2.\end{aligned}$$

Using p_1 and p_2 as in Section 6.4 and proceeding as in Equation (6.5) we get

$$\begin{aligned}|\partial_y(p_1) - \partial_y(p_2)| &< \frac{130 + 56k + 8k^2}{9\sqrt{2}k^2} \\ &<^* \frac{5}{3}(2k-1) - 10 < H_y.\end{aligned}$$

The starred inequality holds for $k \ge 8$. All in all, $\partial_y h(p_2) > 0$ for $k \ge 8$.

6.8 Step 7

First we show that $b_{k+5} \uparrow b_{3k+8}$ throughout Ω_k'. Define

$$g_{52} = \pi_y(b_{k+5}) - \pi_y(b_{3k+8}), \quad h = g_{52} - g_{50}.$$

We will show that $h > 0$ in R_k, which means that $g_{52} > 0$ whenever $g_{50} > 0$, which means that $g_{52} > 0$ on Ω_k'. For $k = 5$ we have this formula for g_{52}:

$$\begin{aligned}&-\cos(-14x-9y) + \cos(-14x-7y) - \cos(-12x-5y) \\ &+\cos(-12x-7y) - \cos(-10x-5y) + \cos(-10x-3y) \\ &-\cos(-8x-y) + \cos(-8x-3y) - \cos(-6x-y) \\ &+\cos(-6x+1y) - \cos(-4x+3y) + \cos(-4x+1y) \\ &-\cos(-2x+3y).\end{aligned}$$

We compute that

$$\begin{aligned}h(x,y) = &\cos(2x-3y) + \cos(4x-3y) - 2\cos(4x-y) \\ &- 2\cos(6x-y) - \cos(y) - \cos(2x+y) \\ &+ \cos(2x+3y) + \cos(4x+3y). \qquad (6\text{–}18)\end{aligned}$$

This holds independent of k, for the same reason as above.

We compute that

$$h(p_\infty) = 0, \quad \nabla h(p_\infty) = (17\sqrt{3}, -\sqrt{3}).$$

Equations (6–18) and (2–3) gives us the absolute bound $|\partial^2 h| < 102$. Using the fact that $R_k \in S_{1/(12k)} \subset S_{1/96}$, our two bounds imply throughout R_k that

$$\partial_x h > 25, \quad \partial_y h > -4.$$

This means that $\nabla h(p)$ has positive dot product with any unit vector emanating from p_∞ and pointing in R_k. (These vectors are all quite close to $(1,-1)/\sqrt{2}$, on account of Condition 2 of Equation (6–3).) Since $h(p_\infty) = 0$ the positive dot product property gives us $h > 0$ on all of R_2.

Now we show that $a_{2k+6} \uparrow a_{3k+7}$ throughout Ω_k'. We define

$$g_{53} = \pi_y(a_{2k+6}) - \pi_y(a_{3k+7}), \quad h = g_{53} - g_{51}.$$

It suffices to prove that h is positive.

We have this formula for g_{53}:

$$\begin{aligned}&-\cos(-16x-9y) + \cos(-16x-11y) - \cos(-14x-9y) \\ &+\cos(-14x-7y) - \cos(-12x-5y) + \cos(-12x-7y) \\ &-\cos(-10x-5y) + \cos(-10x-3y) - \cos(-8x-y) \\ &+\cos(-8x-3y) - \cos(-6x-y).\end{aligned}$$

We compute that

$$h(x) = -2\cos(x)\cos(5x-y)$$

independent of k. We just need to see that $f(x,y) = \cos(5x-y) < 0$ on R_k. We compute

$$f(p_\infty) = 0, \quad \nabla f(p_\infty) = (-5, 1).$$

We have the absolute bound $|\partial^2 f| < 25$ and hence for $x \in R_k$ we get

$$\partial_x f < -4, \quad \partial_y f < 2.$$

The rest of the proof is as in the first part of this step.

7. PROOF OF THEOREM 1.3

7.1 The Limiting Picture

Let $\{T_n\}$ be as in Theorem 1.3. Let v_j denote the vertex whose angle is near $j\frac{\pi}{6}$. We scale our triangles so that $\lim T_n = T_\infty$. The convergence takes place, for example, in the Hausdorff topology on closed planar subsets. Let $\mathcal{T}$ denote the $(2,3,6)$ Euclidean tiling by isometric copies of T_∞. We label the edges and vertices of $\mathcal{T}$ as the edges and vertices of T_∞ are labeled.

It suffices to consider periodic billiard paths represented by even-length words W. Tautologically, W represents a periodic billiard path in T if and only if the first and last sides of $U(W,T)$ are parallel and the interior of $U(W,T)$ contains a line segment L, called a *centerline*, such that L intersects the first and last sides at corresponding points. The orbit tile $O(W)$ consists of those

triangles T for which W represents a periodic billiard path. W is *stable* iff $O(W)$ is an open set, and otherwise *unstable*.

Lemma 7.1. *If W is unstable then $O(W)$ is contained in a line of Δ.*

Proof: If W is unstable then there is a nontrivial condition on the angles, clearly linear, for the parallelism of the first and last sides of $U(W,T)$. □

Lemma 7.2. *T_∞ does not have a stable periodic billiard path.*

Proof: This is a result of Galperin–Stepin–Vorobets [Galperin et al. 91]. See also [Hooper 06], which proves that no right triangle has a stable periodic billiard path. □

No rational line in parameter space contains infinitely many of the points representing our sequence $\{T_n\}$. Hence, if Theorem 1.3 is false then we can find a stable word W such that $T_n \in O(W)$ for all n. Since W is fixed we write $U_n = U(W,T_n)$. Let $\widehat{U}_n$ be the bi-infinite periodic continuation of U_n. Let L_n denote a centerline of U_n and let $\widehat{L}_n$ be the corresponding centerline for $\widehat{U}_n$. We normalize so that $\widehat{L}_n$ is the x-axis. Then the limit $\widehat{L}_\infty$ is also the x-axis. We can take a subsequence such that $\widehat{U}_n$ converges to an infinite union $\widehat{U}_\infty$ of triangles in $\mathcal{T}$.

A *vertex of* $\widehat{L}_\infty$ is a vertex of $\mathcal{T}$ that lies on $\widehat{L}_\infty$. The boundary of $\widehat{U}_\infty$ consists of two infinite polygonal lines, $\widehat{U}_\infty(+)$ and $\widehat{U}_\infty(-)$. Each vertex of $\widehat{L}_\infty$ lies either on $\widehat{U}_\infty(+)$ or on $\widehat{U}_\infty(-)$. We say that the sign of the vertex is $(+)$ or $(-)$ accordingly.

Lemma 7.3. *$\widehat{L}_\infty$ contains an infinite list of vertices of $\mathcal{T}$. Moreover, vertices with both signs must appear on $\widehat{L}_\infty$.*

Proof: If $\widehat{L}_\infty$ contains no vertex of $\mathcal{T}$ then $U(W,T_\infty)$ has a centerline, contradicting Lemma 7.2. Hence $\widehat{L}_\infty$ contains infinitely many vertices by periodicity. If only vertices of one sign appear on $\widehat{L}_\infty$ then we could perturb $\widehat{L}_\infty$ parallel to itself, producing a line that is contained in the interior of the triangles of $\widehat{U}(W,T_\infty)$. But then U_∞ would have a centerline, a contradiction. □

Here is a more subtle result, which we prove in Section 8:

Lemma 7.4. *Suppose that $\widehat{L}_\infty$ has vertices of type* 2*. Then $\widehat{L}_\infty$ contains vertices of odd type as well.*

We label the vertices of $\widehat{L}_\infty$ as $, \ldots, v_\infty(1), v_\infty(2), \ldots$ from left to right. Let $v_n(j)$ denote the vertex of $\widehat{U}_n$ that corresponds to $v_\infty(j)$. Note that $v_n(j)$ need not lie on $\widehat{L}_n$. However, the distance from $v_n(j)$ to $\widehat{L}_n$ converges to 0 as $n \to \infty$. We let $\widehat{Z}_n$ denote the polygonal path whose vertices are $v_n(j)$. We label the vertices of $\widehat{Z}_n$ in the same way that the vertices of $\widehat{L}_\infty$ are labeled. A vertex of $\widehat{Z}_n$ is $(+)$ iff it has positive y coordinate.

FIGURE 26.

Note that $\widehat{Z}_\infty$ is a straight line and $\widehat{Z}_n$ is nearly a straight line. Let $\theta_n(j)$ denote the exterior angle at $v_n(j)$, measured according to the sign conventions of Figure 26. We are going to get our contradiction by analyzing the way $\widehat{Z}_\infty$ bends and interacts with $\widehat{L}_\infty$. Given Lemma 7.4 there are two cases, depending on whether $\widehat{L}_\infty$ has any type-2 vertices. When $\widehat{L}_\infty$ does have some type-2 vertices the situation is much more difficult.

7.2 Case 1: Some Type-2 Vertices

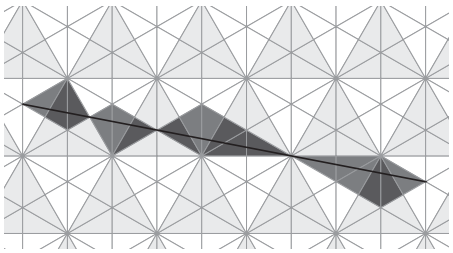

FIGURE 27.

Figure 27 (suitably rotated) shows an example of interest to us. Lemma 7.4 says that $\widehat{L}_\infty$ has vertices of both even and odd type. But then the lattice structure of $\mathcal{T}$ forces a precise structure.

Lemma 7.5. *On $\widehat{L}_\infty$ the pattern of vertex types is $, \ldots, 2, 1, 2, 3, 2, 1, 2, 3, \ldots$. The union of triangles encountered by $\widehat{L}_\infty$ between vertices has rotational symmetry about every odd vertex. The distance between successive vertices of type* 1 *and* 2 *is twice the distance between successive vertices of type* 2 *and* 3*.*

Proof: $\widehat{L}_\infty$ encounters an infinite succession of type-2 vertices, each contained in a white or gray triangle. These colors alternate. Otherwise, $\widehat{L}_\infty$ would encounter (say) two white centers in a row. But then there would be

a translation symmetry of $\widehat{L}_\infty$ taking one white triangle to the next, and there would be no gray centers at all. But since $\widehat{L}_\infty$ encounters some odd vertex, there is a 180-degree rotational symmetry of $\widehat{L}_\infty$, and this symmetry interchanges gray and white. So, the colors alternate. An odd vertex resides halfway between the centers of successive triangle centers of different colors. The odd vertex types alternate because there is *not* 180-degree rotational symmetry about the type-2 vertices. The lengths of successive segments on $\widehat{L}_\infty$ is now forced by the symmetry of $\mathcal{T}$. □

We label the vertices of $\widehat{Z}_n$ so that $v_n(0)$ has type 2 and $v_n(1)$ has type 1. There is some number L such that the asymptotic length of the segments connecting type-1 vertices to type-2 vertices is $2L$ while the asymptotic length of the segments connecting type-2 vertices to type-3 vertices has length L.

The rotational symmetry detailed in Lemma 7.5 implies that the angles about odd vertices are

$$\theta_n(4j+1) = \pm 6\epsilon_n, \quad \theta_n(4j+3) = \pm 2\iota_n. \tag{7–1}$$

To analyze $\theta_n(2j)$ we look carefully at Figure 28, which shows a picture of what $\widehat{Z}_n$ would look like in a neighborhood of $v_n(0)$ if two of the triangles at this spot were removed and the resulting object were bent so that the two external angles (labeled β) coincided. In this position there might be a nonzero bending angle $\pm\delta$ between the two segments S_1 and S_2.

Hence

$$\theta_n(2j) = (-1)^j \delta_n \mp 3\epsilon_n \mp 3\iota_n. \tag{7–2}$$

The signs in front of $3\epsilon_n$ and $3\iota_n$ are the opposite of the label of the vertex, as in Case 3. The reason for the alternation of signs in front of δ_n is that $\widehat{Z}_n$ encounters the centers of the white and gray triangles in $\mathcal{T}$ in alternating fashion. If $\widehat{L}_\infty$ is actually an edge of $\mathcal{T}$ then we would have $\delta_n = 0$.

Lemma 7.6. *There is a constant C, depending only on the combinatorics, such that $|\delta_n| < C\epsilon_n$.*

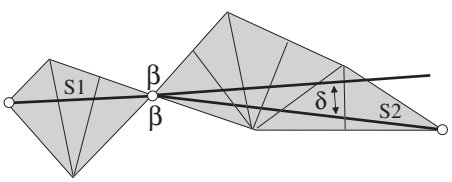

FIGURE 28.

Proof: This follows from the fact that $\iota_n < \epsilon_n$ and that $\phi_n(j)$ is a smooth function of ϵ_n and ι_n that vanishes at $(0,0)$. □

In light of Lemma 7.6 we can pass to a subsequence such that

$$\lim \frac{\delta_n}{\epsilon_n} = D.$$

We introduce the notation $X \sim Y$ to denote that $X = Y$, up to an error that vanishes faster than ϵ does. To save words we will say that such an error is *negligible*. For instance, $\iota_n = 0$ up to a negligible error. In light of Lemma 7.6 we can pass to a subsequence such that

$$\theta_n(4j+1) = \pm 6\epsilon_n, \quad \theta_n(2j) = ((-1)^j D \mp 3)\epsilon_n,$$
$$\theta_n(4j+3) \sim 0.$$

The sign choices are as above.

Say that the *rotation angle* of a vector is the counterclockwise angle in $[0,\pi)$ by which the positive x-axis must be rotated to produce a ray pointing in the same direction as the vector. For $j \equiv 1 \bmod 4$, let $\lambda_n(j)$ denote the angle bisector to $\widehat{Z}_n$ at $v_n(j)$. We think of λ_n as a ray pointing upwards. Let $\phi_n(j)$ be such that the rotation angle of $\lambda_n(j)$ is $\frac{\pi}{2} + \phi_n(j)$. Lemma 7.6 holds for $\phi_n(j)$ and so we can pass to a subsequence such that

$$K_j = \lim_{n\to\infty} \frac{\phi_n(j)}{\epsilon_n}, \quad j = \ldots, 1, 5, 9, \ldots, \tag{7–3}$$

exists. (Actually, we don't really need to pass to a subsequence; the limit exists because ι_n is negligible.)

We normalize our pictures so that $v_n(1)$ lies on the y-axis. If necessary we can apply the map $(x,y) \mapsto (x,-y)$ to our pictures, to guarantee that the first vertex $v_n(1)$ is $(+)$. Let a_1 be the rotation angle of the vector that points from $v_n(1)$ to $v_n(2)$. Next, for indices $j = 2,3,4$ let $a_j = \theta_n(j)$. We have $a_3 \sim 0$. Figure 29 shows a schematic picture of the situation. The actual placement of the vertices and directions of the bends depends on the geometry of the given situation.

Define

$$b_1 = a_1, \quad b_2 = a_1 + a_2, \quad b_4 = a_1 + a_2 + a_4.$$

Then b_j is the rotation angle of the segment pointing from $v_n(j)$ to $v_n(j+1)$.

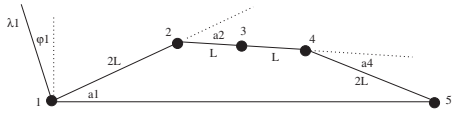

FIGURE 29.

Define

$$c_4 = b_1 + b_2 + b_4 = 3a_1 + 2a_2 + a_4.$$

As $n \to \infty$ all our numbers tend to 0 at least as quickly as ϵ_n tends to 0. Hence $\sin(b_j) \sim b_j$. Let y_j be the y coordinate of the point $v_n(j)$. It follows from trigonometry that

$$\begin{aligned} y_5 - y_1 &= 2L(\sin(b_1) + \sin(b_2) + \sin(b_4)) \\ &\sim 2L(b_1 + b_2 + b_4) = 2Lc_4. \end{aligned}$$

Since $\theta_n(1) \sim 6\epsilon_n$ we have

$$a_1 \sim (3+K_1)\epsilon_n, \quad a_2 \sim (-D-3s_2)\epsilon_n, \quad a_4 \sim (D-3s_4)\epsilon_n.$$

Here $s_2, s_4 \in \{-1, 1\}$ are the signs of $v_n(2)$ and $v_n(4)$. We compute that

$$\begin{aligned} c_4 &= 3a_1 + 2a_2 + a_4 \sim (9 - 6s_2 - 3s_4 + 3K_1 - D)\epsilon_n \\ &\geq (3K_1 - D)\epsilon_n. \end{aligned}$$

If $3K_1 > D$ then $c_4 > 0$ for n sufficiently large. Regardless of the values of K_1 and D we compute

$$b_4 \sim b_1 + (-3s_2 - 3s_4)\epsilon_n. \tag{7–4}$$

When $c_4 > 0$ the point $v_n(5)$ is (+) and

$$b_5 = b_4 + 6\epsilon_n \sim b_1 + (6 - 3s_2 - 3s_4)\epsilon_n \geq b_1. \tag{7–5}$$

Equation (7–5) tells us that $\phi_5 \geq \phi_1$, up to a negligible error. Hence $K_5 \geq K_1$. Also, note that $c_4 > 0$, which makes $y_5 > y_1$. We can now shift indices by 5 and repeat our argument. Iterating, we get $\{y_j\}$ to grow without bound, contradicting periodicity.

Suppose that $3K_1 < D$. We can apply the map $(x, y) \mapsto (-x, y)$ to the picture. This has the effect of negating both K_1 and D, and leads to $3K_1 > D$. Again we have a contradiction.

We must have $3K_1 = D$. This analysis works for $j = 1, 5, 9, \ldots$ and so we must have $3K_j = D$ for all such j. We normalize so that $v_n(1)$ is (+) and $D \geq 0$. Hence $K \geq 0$. Hence, $v_n(2)$ is (+). Hence, in Equation (7–4), we have $s_2 = 1$. If $v_n(5)$ is (−) we have

$$b_5 \sim b_1 + (-6 - 3 - 3s_4)\epsilon_n. \tag{7–6}$$

But $b_5 \sim b_1$ because $K_5 = K_1$. Equation (7–6) is impossible for $s_4 = \pm 1$. Hence $v_n(5)$ is (+). But then Equation (7–5) implies that $s_4 = 1$. Hence $v_n(j)$ is (+) for $j = 1, 2, 3, 4, 5$. Iterating, we see that all vertices are (+). This situation contradicts Lemma 7.3

7.3 Case 2: No Type-2 Vertices

Figure 30, suitably rotated, shows an example of a case of interest to us. We make the same setup as in Case 1; $\widehat{Z}_n$ consists of segments all having the same length and has rotational symmetry about every vertex.

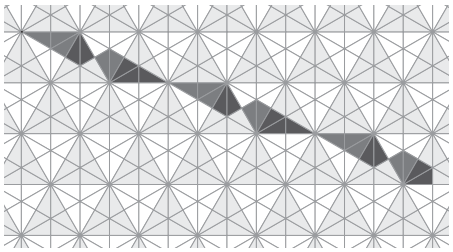

FIGURE 30.

If there are some type-3 vertices, then there must also be some type-1 vertices. We label the vertices by odd integers, so that vertices of type 1 are congruent to 1 mod 4 and vertices of type 3 are congruent to 3 mod 4. This is just as in Case 1, except that there are no even vertices. Equation (7–1) is the same.

We can normalize so that $v_n(1)$ is labeled by a (+). Suppose first that $K_1 \geq 0$. (We are deliberately including the case $K_1 = 0$.) Then $a_1 > 0$ and the segment pointing from $v_n(1)$ to $v_n(3)$ has positive rotation angle. Hence, the segment pointing from $v_n(3)$ to $v_n(5)$ also has positive rotation angle once n is sufficiently large. Hence $v_n(5)$ is (+). Moreover, $K_5 \sim K_1 + 6\epsilon_n$. Iterating we get that $K_9 \sim K_1 + 12\epsilon_n$ and $K_{13} \sim K_1 + 18\epsilon_n$, etc. This growing sequence of K values contradicts the periodicity. If $K_1 \leq 0$ we can apply the map $(x, y) \mapsto (-x, y)$ to return to the case $K_1 \geq 0$. Every case leads to a contradiction.

If there are no type-3 vertices then there are only type-1 vertices. In this case we can make the same argument, using $2\iota_n$ in place of $6\epsilon_n$.

This completes our proof of Theorem 1.3, modulo the proof of Lemma 7.4.

8. PROOF OF LEMMA 7.4

We begin with a well-known stability criterion. Compare [Hooper 06] and [Halbeisen and Hungerbuhler 00].

Lemma 8.1. *Let $W = w_1, \ldots, w_{2n}$. Let n_{dj} denote the number of solutions to the equation $w_i = d$ with i congruent to j mod 2. Let $n_d = n_{d0} - n_{d1}$. Then W is stable iff $n_d(W) = 0$ for $d = 1, 2, 3$.*

Proof: Let T be a triangle. We can find numbers $\alpha_1, \alpha_2, \alpha_3$ such that the jth interior angle of T is $\alpha_{j-1} +$

α_{j+1}. Indices are taken modulo 3. Let $\{T_k\}$ denote the bi-infinite continuation of the unfolding $U(W,T)$. Then T_{2n+k} is obtained from T_k by translating some amount and then rotating by $\sum_{d=1}^{3} 2n_d\alpha_d$. In order for this sum to vanish for every choice of T we must have $n_1, n_2, n_3 = 0$. Conversely, if $n_1, n_2, n_3 = 0$ then the sum always vanishes. In the vanishing case the triangles T_{2n+k} and T_k are always translates of each other, and then the existence of a centerline is an open condition. □

We will suppose that $\widehat{L}_\infty$ has no vertices of odd type and then get a contradiction. We color $\mathcal{T}$ as in Figures 27 and 30. We can assume that $\widehat{L}_\infty$ contains the barycenter of a white triangle. Note that the midpoint of a segment in $\mathcal{T}$ that joins a white barycenter to a gray barycenter also contains a vertex of odd type. Hence $\widehat{L}_\infty$ contains an infinite list of white barycenters, and no gray ones. We let F_∞ denote the portion of L_∞ that connects one white barycenter to the next. The line segment L_∞ consists of k consecutive copies of F_∞ for some positive integer k.

Recall that L_n is a centerline of $U(W,T_n)$, and that L_∞ is the limit of L_n. We cannot unambiguously determine the word W from L_∞ (or $\widehat{L}_\infty$) because we don't know what L_n does near the vertices. However, away from the vertices we know what L_n must do. Let w denote the word consisting of edges crossed by the interior of F_∞. Let ϵ_j stand for either the word 131 or 313. Then W must have the form $(w\epsilon_1)(w\epsilon_2)\dots(w\epsilon_k)$.

Let $|w|$ be the length of w. We move F_∞ parallel to itself by a small amount. The resulting segment intersects $|w|+3$ edges, and has endpoints in two triangles that are translation equivalent, so $|w|+3$ is even. Hence $|w|$ is odd. Since $|\epsilon_j|$ is also odd, $|w|+|\epsilon_j|$ is even. Hence

$$n_2(W) = \sum_{j=1}^{k} n_2(w\epsilon_j) = kn_2(w).$$

Here n_2 is the same quantity as in Lemma 8.1. Since W is stable we have $n_2(W) = 0$ by Lemma 8.1. Hence $n_2(w) = 0$. To get a contradiction, we just have to show that $n_2(w) \neq 0$.

Say that a line of $\mathcal{T}$ is *thick* if it contains no vertices of type 3. Since F_∞ starts and ends in a white triangle, F_∞ crosses the thick edges altogether an even number of times. There are three families of parallel thick edges and we can ask about how many times F_∞ crosses each of the families.

Lemma 8.2. *F_∞ crosses two of the families an odd number of times.*

Proof: Applying an affine automorphism we can identify the centers of the white triangles with $\mathbb{Z}\times\mathbb{Z}$. We can think of F_∞ as connecting the point $(0,0)$ to the point (m,n) with m and n relatively prime. Hence, not both m and n can be even. But m and n represent two of the three numbers of interest to us. Hence, at least one of the numbers of interest to us is odd. Since the sum of the three numbers is even, exactly two of them are odd. □

The translation symmetry group G of $\mathcal{T}$ acts on $\mathbb{R}^2$, so that the quotient is a torus. The union of two triangles, white and gray, serves as a fundamental domain. Let X denote the square torus. Let $L \subset X$ be the image of $\widehat{L}_\infty$ under the map

$$\mathbb{R}^2 \stackrel{\pi}{\to} \mathbb{R}^2/G \stackrel{A}{\to} X.$$

Here π is the quotient map and A is a locally affine map. Compare the proof of Lemma 8.2.

The triangulation of $\mathcal{T}$ induces a triangulation of X: First X is subdivided into two triangles and then these triangles are barycentrically subdivided. Figure 31 shows the picture, with the little triangles alternately colored black and white. L contains one of the barycenters of X, but no other vertices of the triangulation.

The *thick edges* are the ones present before the barycentric subdivision. Each time L intersects a thick edge we can say whether L crosses from black to white or from white to black. We define $n_2(L)$ as the number of black-to-white crosses minus the number of white-to-black crosses. We have $n_2(L) = 2$ for the example shown in the right-hand side of Figure 31. By construction we have $n_2(L) = n_2(w)$. We just need to show that $n_2(L) \neq 0$ in general.

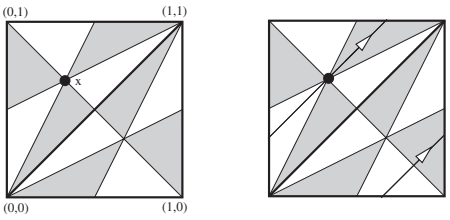

FIGURE 31.

Let V denote the left vertical edge of X and let H denote the top horizontal edge. Let D denote the diagonal edge. From Lemma 8.2 we know that L intersects two of H, V, D an odd number of times, and the remaining edge an even number of times. There is an affine automorphism of X that preserves x and cycles H, V, D. Thus, we can assume that L intersects H and V an odd number of times, and D an even number of times. The points of

$L \cap D$ are evenly spaced on D and so half of them occur on the left of the center point and the other half occur on the right. Hence $n_2(L)$ can be determined just from the intersections of L with H and V.

Let $\{L_t |\ t \in [0,1]\}$ denote the continuous family of loops parallel to $L = L_0$. Let s be a parameter such that L_s contains the midpoint of H. The points of $L_s \cap H$ are odd in number and evenly spaced about $L_s \cap H$. Hence $H \cap V \notin L_s$. By symmetry the points of $L \cap V$ are evenly spaced about the midpoint of V. Since $H \cap V \notin L_s$ the midpoint of V is contained in L_s. In short, L_s contains the midpoints of both H and V, and neither endpoint.

By symmetry $n_2(L_s) = 0$. (Here we ignore the crossings at the midpoints.) From the pattern of the colorings we see that $n_2(L_t) = \pm 2$ if t is sufficiently close to s. However, we can choose s so that L_t crosses no vertices of ∂X for $t \in [0, s)$. Hence $n_2(L_0) = \pm 2$.

We have shown that $n_2(w) \neq 0$. This contradiction completes our proof of Lemma 7.4.

ACKNOWLEDGMENTS

I would like to thank Pat Hooper, Curt McMullen, Martin Schmoll, Serge Tabachnikov, and Serge Troubetzkoy for helpful and interesting conversations related to billiards. I would especially like to thank Pat, who is my collaborator on McBilliards. Finally, I would like to thank the Max Planck Institute in Bonn, and the University of Bonn, for providing a stimulating environment in which the results of this paper were discovered.

This research was supported by N.S.F. Grant DMS-0305047, by a Guggenheim Fellowship, and by the Ruth M. Davis Endowment.

REFERENCES

[Boshernitzyn et al. 98] M. Boshernitzyn, G. Galperin, T. Kruger, and S. Troubetzkoy. "Periodic Billiard Trajectories Are Dense in Rational Polygons." *Trans. AMS* 350 (1998), 3523–3535.

[Galperin et al. 91] G. A Galperin, A. M. Stepin, and Y. B. Vorobets. "Periodic Billiard Trajectories in Polygons." *Russian Math Surveys* 47 (1991), 5–80.

[Gutkin 96] E. Gutkin. "Billiards in Polygons: Survey of Recent Results." *J. Stat. Phys.* 83 (1996), 7–26.

[Halbeisen and Hungerbuhler 00] L. Halbeisen and N. Hungerbuhler. "On Periodic Billiard Trajectories in Obtuse Triangles." *SIAM Review* 42:4 (2000), 657–670.

[Holt 98] F. Holt. "Periodic Reflecting Paths in Right Triangles." *Geometriae Dedicata* 46 (1993), 70–93.

[Hooper 06] W. P. Hooper. "Periodic Billiard Paths in Right Triangles Are Unstable." To appear in *Geometriae Dedicata*, 2006.

[Masur 86] H. Masur. "Closed Trajectories for Quadratic Differentials with an Application to Billiards." *Duke Math. J.* 53 (1986), 307–314.

[Masur and Tabachnikov 02] H. Masur and S. Tabachnikov. "Rational Billiards and Flat Structures." In *Handbook of Dynamical Systems 1A*, edited by B. Hassleblatt and A. Katok, 2002.

[Schwartz 05a] R. Schwartz. "Obtuse Triangular Billiards II: 100 Degrees Worth of Periodic Billiard Trajectories." Preprint, 2005.

[Schwartz 05b] R. Schwartz. "Web McBilliards Homepage." Available online at www.math.brown.edu/~res/Billiards/index.html, 2005.

[Tabachnikov 95] S. Tabachnikov. "Billiards." *SMF Panoramas et Syntheses* 1 (1995).

[Troubetzkoy 04] S. Troubetzkoy. "Billiards in Right Triangles." Preprint, 2004.

[Veech 92] W. Veech. "Teichmüller Curves in Moduli Space: Eisenstein Series and an Application to Triangular Billiards." *Invent. Math.* 97 (1992), 341–379.

[Wolfram 00]] S. Wolfram. *Mathematica: A System for Doing Mathematics by Computer*. Wolfram Press, 2000.

Richard Evan Schwartz, Department of Mathematics, Brown University, Providence, RI 02912 (res@math.brown.edu)

Received May 9, 2005; accepted September 20, 2005.